Molecular Genetics and Genomics (2025) 300:30
https://doi.org/10.1007/s00438-025-02237-7

ORIGINAL ARTICLE

Construction of a prognostic risk model for clear cell renal cell carcinomas based on centrosome amplification-related genes

Bingru Zhou[1,3] · Fengye Liu[3] · Ying Wan[3] · Lin Luo[1,3] · Zhenzhong Ye[1,2] · Jinwei He[3] · Long Tang[3] · Wenzhe Ma[1] · Rongyang Dai[1,2,3]

Received: 30 November 2024 / Accepted: 25 February 2025
© The Author(s) 2025

Abstract

Clear cell renal cell carcinoma (ccRCC) is the urological malignancy with the highest incidence, centrosome amplification-associated genes (CARGs) have been suggested to be associated with carcinogenesis, but their roles in ccRCC are still incompletely understood. This study utilizes bioinformatics to explore the role of CARGs in the pathogenesis of ccRCC and to establish a prognostic model for ccRCC related to CARGs. Based on publicly available ccRCC datasets, 2312 differentially expressed genes (DEGs) were identified (control vs. ccRCC). Disease samples were classified into high and low scoring groups based on CARG scores and analysed for differences to obtain 345 DEGs associated with CARG scores (S-DEGs). 137 candidate genes were obtained by taking the intersection of DEGs and S-DEGs. Six prognostic genes (PCP4, SLN, PI3, PROX1, VAT1L, and KLK2) were then screened by univariate Cox, LASSO, and multifactorial Cox regression. These genes exhibit a high degree of enrichment in ribosome-associated pathways. Both risk score and age were independent prognostic factors, and the Nomogram constructed based on them had a good predictive performance (AUC > 0.7). In addition, immunological analyses identified 6 different immune cells and 23 immune checkpoints between the high- and low-risk groups, whereas mutational analyses identified frequent VHL mutations in both high- and low-risk groups. Finally, 93 potentially sensitive drugs were identified. In conclusion, this study identified six CARGs as prognostic genes for ccRCC and established a risk model with predictive value. These findings provide insights for prognostic prediction of ccRCC, optimisation of clinical management and development of targeted therapeutic strategies.

Keywords Clear cell renal cell carcinomas · Centrosome amplification-related genes · Prognostic genes · Risk model

Introduction

Renal cell carcinoma (RCC) is a common malignancy, accounting for approximately 4% of all cancers and nearly half of urinary tract cancers (Shi et al. 2023; Siegel et al. 2021). Clear cell renal cell carcinoma (ccRCC), the most prevalent subtype, comprises 70–80% of RCC cases (Shuch et al. 2015). Characterized by clear cell morphology resulting from lipid and glycogen accumulation, ccRCC cells also exhibit irregular nuclei and abnormal chromatin, distinguishing them microscopically (Muglia and Prando 2015). Despite significant advances in the molecular understanding of ccRCC, critical gaps persist, particularly in the areas of metabolic reprogramming during tumor progression and resistance to therapy. ccRCC exhibits the Warburg effect (aerobic glycolysis) and alterations in lipid metabolism, which supports tumor growth under hypoxic conditions and contributes to immune evasion and resistance (Wettersten

Communicated by Wenfei Jin.

✉ Wenzhe Ma
wzma@must.edu.mo

✉ Rongyang Dai
dryrun2502@163.com

1 State Key Laboratory of Quality Research in Chinese Medicine, Faculty of Chinese Medicine, Macau University of Science and Technology, Macau, China

2 Department of Biochemistry and Molecular Biology, School of Basic Medicine and Forensic Medicine, North Sichuan Medical College, Nanchong, China

3 School of Basic Medical Sciences, Southwest Medical University, Luzhou, China

Published online: 13 March 2025

et al. 2017) (Makhov et al. 2018). In addition, mutations in the VHL gene are a hallmark of ccRCC (Tan et al. 2023), with VHL inactivation causing overproduction of vascular endothelial growth factor (VEGF), leading to excessive angiogenesis (Ding et al. 2024). These characteristics increase the complexity and treatment difficulty of ccRCC. Although novel immunotherapies and combination strategies have improved the prognosis of some patients, effective treatment options remain limited. Therefore, there is an urgent need to identify new biomarkers and explore more effective treatment strategies. Furthermore, ccRCC has a high recurrence rate and low survival rate (Noone et al. 2017), making early detection and intervention crucial. The exploration of prognostic models holds promise in addressing this challenge. This study aims to use bioinformatics to explore the mechanisms of ccRCC and establish more accurate prognostic models to improve clinical management and treatment strategies.

Centrosome amplification (CA) refers to abnormalities in the size, number, and localization of centrioles, leading to distorted centrosome morphology (Godinho et al. 2014; Prakash et al. 2023). CA can be observed in various cancers and is associated with poor clinical outcomes, such as higher tumor grade, recurrence, and metastasis (Mittal et al. 2021). As tumors progress, the level of CA increases; normal tissues exhibit the lowest CA levels, while invasive tumors have the highest (Zhao et al. 2021). This suggests that CA promotes tumor evolution and metastasis by enhancing cell invasion and increasing metastatic potential. Additionally, CA is closely linked to genomic instability, which can trigger chromosomal deletions, replication errors, and translocations, leading to mutations in key tumor suppressor genes and oncogenes. This instability further drives tumorigenesis (Saunders 2005). Studies have pointed out that the overexpression of centrosomal replication proteins accelerates CA, resulting in centrosome dysfunction and mitotic disturbances, including improper chromosome separation and changes in gene copy numbers (Vitre and Cleveland 2012; Zhang et al. 2023a). These genetic changes may bypass normal growth-regulatory mechanisms, such as cell cycle checkpoints and apoptosis, leading to malignant transformation. In cancers like breast cancer, CA causes chromosomal instability, making the tumor more aggressive (Denu et al. 2016).

Leucine zipper tumor suppressor 2 (LZTS2) is a potential tumor suppressor gene associated with centrosome amplification in ccRCC and upregulation of LZTS2 is correlated with poor prognosis in ccRCC(Peng et al. 2022). Studies show that LZTS2 colocalizes with gamma-tubulin, MKLP1, and p80 katanin at the centrosomes of mitotic cells and serves as a regulator of microtubule severing at centrosomes (Sudo and Maru 2007, 2008). Abnormalities in LZTS2 may affect centrosome replication and stability. In conclusion, CA and the genomic instability it induces have become central factors in promoting cancer progression, particularly in cancers where CA levels are significantly elevated. CA is considered a highly promising therapeutic target in such cancers (Anderhub et al. 2012; Bose and Dalal 2019). Therefore, a deeper exploration of the development mechanisms of CA in ccRCC will not only enhance our understanding of this disease process but also provide valuable insights for ccRCC diagnosis and prognosis evaluation.

This study investigates centrosome amplification-related genes (CARGs) in ccRCC using transcriptomic data from public databases and existing literature. Prognostic genes were identified through univariate Cox regression, LASSO regression, and multivariate Cox regression to construct and validate a prognostic model. Further analyses, including gene set enrichment analysis (GSEA), immune infiltration, immunotherapy sensitivity, mutation landscape, and transcription factor regulatory networks, were conducted to explore the molecular mechanisms of the selected prognostic genes. These findings offer valuable contributions to clinical diagnosis and prognosis for ccRCC, emphasizing the critical role of CARGs and providing a foundation for future personalized treatment strategies.

Materials and methods

Data extraction

RNA-seq expression profiles, along with clinical feature data (age, stage, gender, tumor-node-metastasis (TNM) stage, and somatic mutations) for 603 ccRCC samples, were retrieved from The Cancer Genome Atlas (TCGA)-KIRC dataset on July 15, 2024 (https://portal.gdc.cancer.gov/). The dataset comprised 527 ccRCC samples and 72 controls, excluding 4 ccRCC samples without survival information. The TCGA-KIRC dataset was designated as the training set. Both expression profiles and clinical data were utilized for gene identification and risk model development (Xiao et al. 2020). Additionally, the GSE29609 dataset (GPL1708 platform) was obtained from the Gene Expression Omnibus (GEO) database (https://www.ncbi.nlm.nih.gov/geo/), consisting of 39 ccRCC patient samples, and used as a validation set. Furthermore, 134 CARGs were sourced from a published study(Liu et al. 2024c).

Data processing

For the training set TCGA-KIRC, the counts data in it were first processed by inverse log2 transformation and rounding, and then the counts and FPKM data containing only

the genes encoding proteins (mRNA) were filtered out. For the validation set GSE29609, the annotation information of the genes was first obtained using the idmap function of the AnnoProbe package (v 0.1.0) (Zeng 2019), and then the mean values of the expression were sorted from largest to smallest, and only the first probe data of its expression was retained for each gene, which avoids the redundancy of data introduced by the duplicate probes. Finally, genes with expression less than 0 and non-coding were removed.

Characterization of candidate genes

First, differentially expressed genes (DEGs) between ccRCC and control groups were identified in the training set using the "DESeq2" (v 1.38.0) package (Love et al. 2014) with thresholds of$|\log_2$Fold Change (FC)$| > 2$ and p.adj<0.05. DEGs, along with the top 10 upregulated and downregulated genes, were visualized using the "ggplot2" (v 3.4.1) and "pheatmap" (v 1.0.12) packages, respectively(Gu 2022) (Zhang et al. 2023d). Next, variations in CARG expression between ccRCC and control groups were assessed *via* single-sample gene set enrichment analysis (ssGSEA) using the "GSVA" (v 1.42.0) package(Liu et al. 2021). Each CARG was scored, and the Wilcoxon test ($p<0.05$) was used to compare the ssGSEA scores of CARGs between ccRCC and control groups. To assess differences in survival rates of ccRCC samples in the training set, disease samples were categorized into high and low-scored groups based on the best cut-off value of the CARG score. The "survival" package (v 3.5.3)(Liu et al. 2021) was used to plot Kaplan-Meier (KM) survival curves for the high- and low-scored groups, with the Log-rank test applied to assess survival differences. Following this, the "DESeq2" (v 1.38.0) package was used to identify S-DEGs between the high- and low-scored groups ($|\log_2$FC$| > 1$, p.adj<0.05), which were visualized using the "ggplot2" (v 3.4.1) package. DEGs and S-DEGs were intersected using the "ggvenn" package (v 0.1.9)(Gao et al. 2024) to identify candidate genes for subsequent analysis.

Enrichment analyses of candidate genes

To explore the functions and involved pathways of the candidate genes, Gene Ontology (GO) and Kyoto Encyclopedia of Genes and Genomes (KEGG) enrichment analyses were performed using the "clusterProfiler" package (v 4.7.1003) (Wu et al. 2021), with significance set at adj.$p<0.05$. The GO analysis included three components: biological processes (BPs), cellular components (CCs), and molecular functions (MFs). The GO results were ranked in descending order based on the number of enriched genes, and the top 5 results from each GO category, along with the top 10 most significantly enriched KEGG pathways (ordered by p-value), were presented.

Identification of prognostic genes and construction of risk model

To identify genes associated with the prognosis of patients with ccRCC in candidate genes, samples with survival information less than 90 days were excluded from both the training and validation sets, leaving 498 samples in the training set and 37 samples in the validation set. Prognostic genes were identified, and a risk model was developed in the training set through a three-step analysis. First, univariate Cox regression analysis was conducted on the candidate genes using the "coxph" function in the "survival" package (v 3.5.3)(Liu et al. 2021), applying criteria of hazard ratio (HR)$\neq 1$ and $p<0.2$. Next, the proportional hazards (PH) assumption test was performed for the genes identified by univariate Cox regression; genes with $p>0.05$ were excluded from further analyses. The remaining genes were then subjected to least absolute shrinkage and selection operator (LASSO) regression using the "glmnet" package (v 4.1-4)(Friedman et al. 2010), with 10-fold cross-validation. The optimal model was selected based on the minimum model error, corresponding to the lambda value, $\text{lambda}_{\text{min}}$. Finally, multivariate Cox regression analysis was applied to the genes from the previous steps using the "survival" package (v 3.5.3), with genes having $p<0.05$ and meeting the PH assumption ($p>0.05$) considered as prognostic markers. The resulting coefficients from the multivariate Cox regression were used to develop the risk model *via* the following formula:

$$score = \sum_{(i=1)}^{n} \beta_i * x_i$$

In this equation, β denotes the risk coefficients for each prognostic gene, and x represents the expression level of each gene.

Validation of the risk model

After developing the risk model, patients with ccRCC were categorized into high-risk and low-risk groups based on the risk score and optimal threshold in both the training and validation sets. To validate the model, risk curves and survival plots were generated for each patient using the "ggplot2" package (v 3.4.1). KM curves for the two risk groups were plotted using the "survival" package (v 3.5.3), and survival differences between the groups were assessed *via* the Log-rank test ($p<0.05$). The accuracy of

the risk prediction was evaluated by plotting receiver operating characteristic (ROC) curves using the "survivalROC" package (v 0.4.9) (Zhang et al. 2023c) in both datasets, with survival time points at 1, 2, and 3 years. An area under the curve (AUC) greater than 0.6 indicated good predictive performance. Additionally, heatmaps were generated using the "pheatmap" package (v 1.0.12) to display the expression of prognostic genes across both risk groups.

Correlation analysis between risk score and clinical features along with independent prognostic analysis

To investigate the distribution of risk scores across subgroups defined by clinical features and evaluate the predictive power of the risk score for these features, KM curves generated by the "survival" package (v 3.5.3) were used to assess differences between the risk groups for each clinical feature ($p<0.05$). Univariate and multivariate Cox regression analyses ($p<0.05$), along with the PH assumption test ($p>0.05$), were performed to determine whether the risk score is an independent prognostic factor and to identify other independent prognostic factors using the "survival" package (v 3.5.3) in the training set. Results were visualized with the "forestplot" package (v 3.1.1) (Jiang et al. 2021), and independent prognostic factors were used to develop a nomogram.

Nomogram establishment and validation

Based on independent prognostic factors, the 1-, 2-, and 3-year mortality rates in the training set were considered as outcome events, and a nomogram was developed using the "rms" (v 6.5) package(Liu et al. 2021). For mortality risk prediction, the nomogram assigned individual scores to each variable based on its value, and the total score was the sum of the individual scores. The total points corresponded to the mortality probability (Pr), with higher total scores indicating a higher risk of mortality. Calibration curves were generated using the "rms" (v 6.5) package, while ROC curves and decision curve analysis (DCA) were performed using the "survivalROC" (v 0.4.9) and "rmda" (v 1.6) packages(Liu et al. 2024a) to evaluate the nomogram's predictive accuracy and effectiveness.

Gene set enrichment analysis (GSEA)

To explore the potential biological functions of the prognostic genes in ccRCC progression, the "psych" package (v 2.4.6) (Kasyanov et al. 2023) was used to calculate correlation coefficients for each prognostic gene against all other genes in the training set (high-risk vs. low-risk). Genes were ranked according to their coefficients. Subsequently, GSEA was performed using the "clusterProfiler" package (v 4.7.1003) ($p<0.05$ and false discovery rate [FDR]<0.25), with the "c2.cp.kegg.v7.4.symbols.gmt" dataset from the Molecular Signatures Database (MSigDB) (http://www.gsea-msigdb.org/gsea/msigdb/index.jsp) serving as the reference. The top five most significantly enriched pathways were reported, ordered by p-value.

Immune infiltration and differential immune checkpoint analysis

To investigate the distribution of immune cell infiltration in both risk groups, the "CIBERSORT" algorithm in the "IOBR" package (v 0.99.8) (Zhang et al. 2024) was used to assess the relative proportions of 22 immune cell types(Chen et al. 2019a) in the training set. The Wilcoxon test was then applied to identify differential immune cell distributions between the two risk groups ($p<0.05$), excluding cells that exhibited immune infiltration in less than 50% of samples. Spearman correlation analysis was conducted using the "psych" package (v 2.4.6) (Kasyanov et al. 2023) to explore the relationship between differential immune cells and prognostic genes (|correlation (cor)| > 0.3, $p<0.05$). To further assess the correlation between risk score and immune checkpoints, the expression levels of 48 immune checkpoints(Hu et al. 2021) were compared between the two risk groups using the Wilcoxon test, and Spearman analysis was also performed to explore the relationship between differential immune checkpoints and prognostic genes (|cor| > 0.3, $p<0.05$).

Mutation analysis

To examine tumor mutation burden (TMB) and the impact of immune checkpoint inhibitors (ICI) therapy, somatic mutation data from the ccRCC training set were analyzed to determine mutation rates in both risk groups. The top 20 mutated genes and 10 mutation types were visualized using the "oncoplot" function in the "maftools" package (v 2.18.0) (Xu et al. 2021). Additionally, survival differences between high and low TMB score groups were explored.

Transcription factor (TF)-mRNA regulatory network construction

For the identification of potential TFs regulating the expression of prognostic genes, these genes were imported into the NetworkAnalyst database (https://www.networkanalyst.ca/) for TF prediction, with the aim of revealing how these transcription factors affect prognostic gene expression, thus providing clues for further functional studies. The TF-mRNA

regulatory network was constructed using "Cytoscape" (v 3.7.2)(Shannon et al. 2003).

Drug sensitivity analysis

To further evaluate the chemotherapeutic response of patients with ccRCC in the training set, the "pRRophetic" package (v 0.5) (Yan et al. 2022) was used to calculate the half-maximal inhibitory concentration (IC_{50}) values for 138 common chemotherapy drugs. Drug information was sourced from the Genomics of Drug Sensitivity in Cancer database (GDSC, https://www.cancerrxgene.org/). The top 10 drugs with significantly higher or lower IC_{50} values between the two risk groups were visualized using the "ggplot2" package (v 3.4.1).

Statistical analysis

All bioinformatics analyses were conducted using "R" software (v 4.2.2), with a significance threshold of $p<0.05$.

Results

A total of 137 candidate genes were characterized

In the training set, a total of 2,312 DEGs were identified between ccRCC and control groups, consisting of 1,500 up-regulated genes (e.g., PAEP, ADAM18, SLC18A3) and 812 down-regulated genes (e.g., SLC12A1, AQP2, UMOD) (Fig. 1a). The density and expression levels of these genes in ccRCC and control groups are shown in Fig. 1b. Additionally, ssGSEA scores of CARGs were significantly higher in the control group (Fig. 1c). Based on the median ssGSEA scores, ccRCC samples in the training set were categorized into high and low-scored groups. Kaplan-Meier analysis revealed that the survival rate of the low-scored group was significantly higher than that of the high-scored group (Fig. 1d). A total of 345 S-DEGs were identified between the high and low-scored groups, including 22 up-regulated genes (e.g., CASP14, REG1B, SP8) and 323 down-regulated genes (e.g., KLK1, HHATL, RHCG) (Fig. 1e). Ultimately, 137 candidate genes were selected through the intersection of the 2,312 DEGs and 345 S-DEGs (Fig. 1f).

Enrichment results of candidate genes

Following the identification of candidate genes, a series of functional analyses were conducted. The candidate genes were enriched in 241 Gene Ontology (GO) terms, including 157 BPs, 22 CCs, and 62 MFs. The most significantly enriched BPs included sodium ion transport and regulation of body fluid levels, while the most enriched CCs were apical part of the cell and apical plasma membrane. Key MFs included active transmembrane transporter activity and monoatomic ion channel activity (Fig. 2a). In KEGG pathway analysis, 125 entries were significantly enriched (Fig. 2b), with pathways such as the synaptic vesicle cycle and collecting duct acid secretion predominating. These results highlighted the importance of transmembrane transport and transporter proteins, suggesting that candidate genes might regulate ccRCC progression by influencing transmembrane transport mechanisms.

A total of six prognostic genes were identified for risk model construction

A univariate Cox regression analysis was conducted on the 137 candidate genes in the training set, yielding 42 genes with significant prognostic value (e.g., CA10, SLC9A4, RP11.35N6.1) (Fig. 3a). Of these, 41 genes passed the PH assumption test ($p>0.05$) and were considered for further analysis (Table 1). LASSO regression with a $lambda_{min}$ value of 0.02309276 ($log_{(Lambda)}$ = -3.768236) identified 19 genes (PAGE2, PI3, FXYD4, HSD11B2, SLN, RAB25, VAT1L, MAGEC3, SBSN, KLK2, SCNN1A, GPR110, PROX1, MAGEC2, ITIH1, CWH43, REG1B, PCP4, and RP11.35N6.1) (Fig. 3b, c). Multivariate Cox regression analysis revealed that six genes (PCP4, SLN, PI3, PROX1, VAT1L, and KLK2) had p-values <0.05 (Fig. 3d), and all passed the PH assumption test ($p>0.05$). These six genes were thus classified as prognostic markers, with PCP4 serving as a protective factor and the remaining five genes (SLN, PI3, PROX1, VAT1L, and KLK2) acting as risk factors. A risk model was subsequently developed, with each patient with ccRCC assigned a risk score based on the coefficients derived from the multivariate Cox regression analysis: risk score = PCP4 × (-0.47089) + SLN × (0.17315) + PI3 × (0.21661) + PROX1 × (0.61581) + VAT1L × (0.25467) + KLK2 × (1.81717).

Risk model has been verified

In both the training and validation sets, risk scores for each patient with ccRCC were computed. Based on the optimal cutoff values (training set: 0.01661667, validation set: -0.4392974), patients with ccRCC were stratified into high-risk and low-risk groups (Fig. 4a, b). A positive correlation was observed between increasing risk scores and higher mortality rates (Fig. 4c, d). Survival analysis revealed significant differences in survival rates between the two groups in both datasets ($p<0.05$), with patients in the high-risk group exhibiting poorer survival outcomes (Fig. 4e, f). The 1-, 2-, and 3-year ROC curve AUCs exceeded 0.6 in both

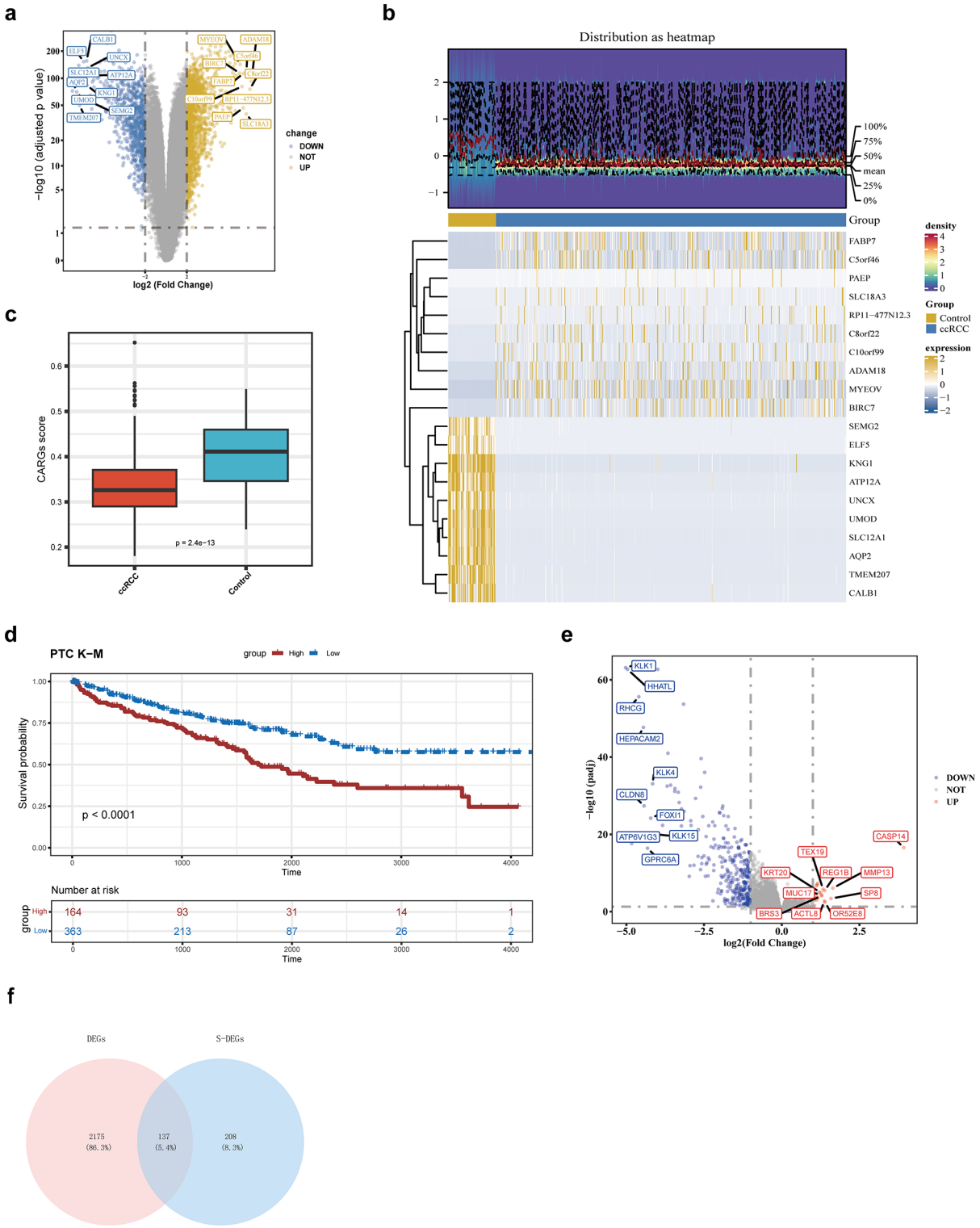

Fig. 1 A total of 137 candidate genes were characterized. **a** Volcano plot of differential genes between ccRCC and control groups. **b** Heat map of differential gene expression between ccRCC and control groups. **c** Box plots of differences in CARGs scores between ccRCC and control groups. **d** CARGs scores in high and low scoring groups survival differences. **e** Differential gene volcano plots between high and low scoring groups. **f** Obtain a Venn diagram of the candidate gene

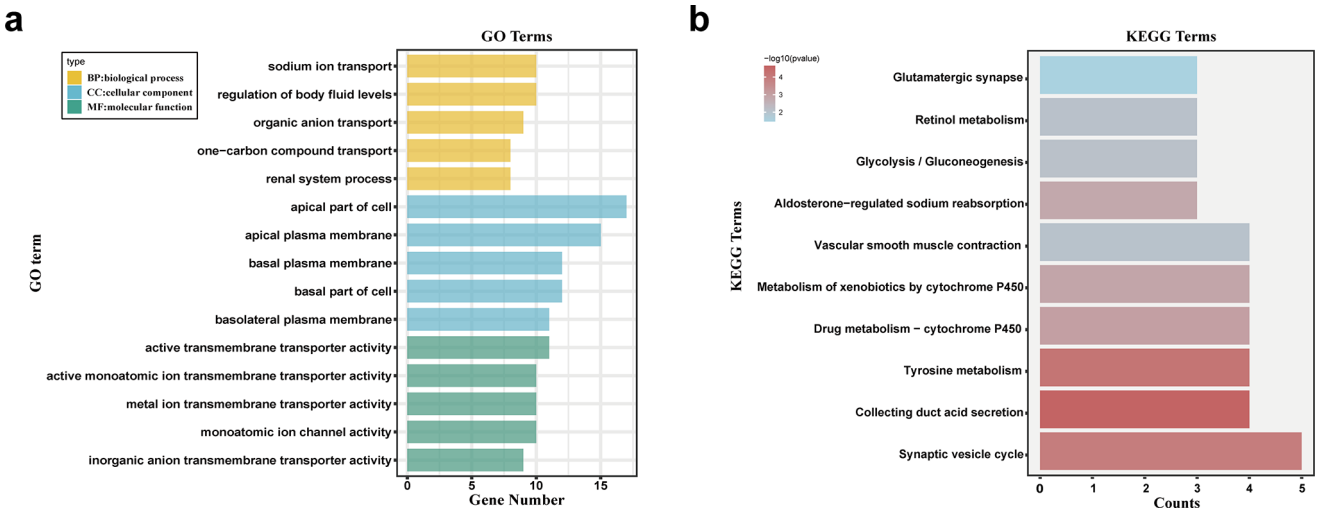

Fig. 2 Functional analyses of candidate genes. **a** GO enrichment analysis of candidate genes. Yellow, blue, and green represent biological processes, cellular components, and biological functions, respectively. **b** Candidate gene KEGG enrichment analysis. Redder colours indicate greater significance

sets, confirming the model's predictive accuracy (Fig. 4g, h). Heatmap analysis indicated significantly higher expression levels of SLN, PI3, PROX1, KLK2, and VAT1L in the high-risk group, while PCP4 expression was elevated in the low-risk group of the training set (Fig. 4i). These findings were similarly observed in the validation set (Fig. 4j).

Relationship between risk score and clinical features as well as evaluation of independent prognostic factors

Risk scores differed significantly across subgroups categorized by T stage (T1-3), M stage (M0-1), clinical stage (2–4), gender, and age (≤60 vs. > 60), as determined by Kaplan-Meier curve analysis (Fig. 5a). Patients with low-risk scores consistently exhibited higher survival rates across all clinical subgroups. Univariate Cox regression analysis revealed significant associations between risk score, age, stage, T stage, and M stage with patient prognosis ($p<0.05$) (Fig. 5b), though stage, T stage, and M stage did not pass the proportional hazards assumption ($p<0.05$) and were excluded. Ultimately, risk score and age, both of which passed multivariate Cox regression analysis ($p<0.05$), were identified as independent prognostic factors (Fig. 5c).

Nomogram development and validation

A nomogram was constructed to predict the 1-, 2-, and 3-year mortality rates of patients with ccRCC (Fig. 6a), with predictions based on total points. The clinical utility of the nomogram was further assessed using calibration curves, ROC curves, and DCA. Calibration curves showed close alignment with the ideal curve for all time points. ROC curve AUCs were ≥0.7, and DCA curves indicated that all factors were above the "All" diagonal line and the "None" horizontal line, indicating satisfactory clinical prediction performance (Fig. 6b-d).

GSEA results

GSEA of prognostic genes in the training set was performed to elucidate their potential functions between the two risk groups. Among these, PCP4 was primarily enriched in oxidative phosphorylation, cardiac muscle contraction, and spliceosome pathways, with all pathways showing upregulation except for spliceosome (Fig. 7a). SLN was predominantly enriched in complement and coagulation cascades, ribosome, and valine, leucine, and isoleucine degradation pathways, with upregulation in all pathways except for the latter (Fig. 7b). KLK2 showed significant enrichment in olfactory transduction, focal adhesion, and renal cell carcinoma pathways (Fig. 7c), suggesting a strong association with ccRCC, with downregulation observed in all pathways except for olfactory transduction. PL3 exhibited upregulation in ribosome and cytokine-cytokine receptor interaction pathways, while showing downregulation in valine, leucine, and isoleucine degradation, propanoate metabolism, and fatty acid metabolism (Fig. 7d). VAT1L was enriched in the calcium signaling pathway and focal adhesion, with downregulation in lysosome, peroxisome, and porphyrin and chlorophyll metabolism (Fig. 7e). Finally, GSEA of PROX1 revealed downregulation in all pathways, including ribosome, oxidative phosphorylation, and three disease-related pathways (Fig. 7f). Notably, four genes—KLK2, PI3, PROX1, and SLN—were all enriched in the ribosome

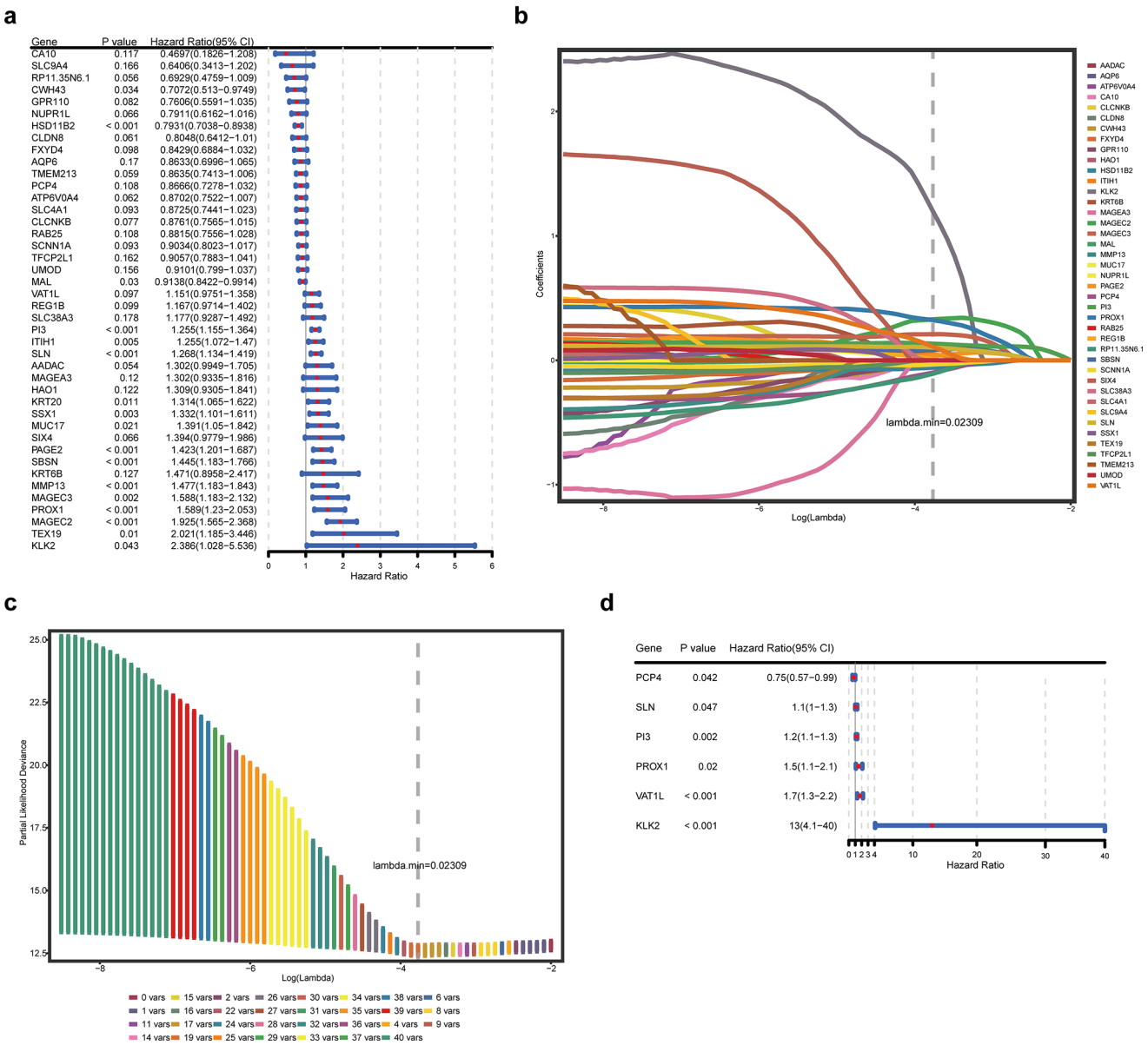

Fig. 3 A total of 6 prognostic genes were obtained. **a** Univariate Cox regression analysis based on candidate genes and forest plotting. **b** Plot of gene coefficients for LASSO analysis, **c** Cross-validation error plot for LASSO analysis. **d** Screening of prognostic genes by multivariate Cox regression and mapping of forests

pathway, suggesting that these prognostic genes may exert their functions through the regulation of ribosomal activity.

A total of six types of differential immune cells and 23 differential immune checkpoints were identified

The distribution and proportion of 22 immune cell types in the high- and low-risk groups of the training set are presented in Fig. 8a, with M2 macrophages showing the highest proportion in both groups. Following exclusion of seven immune cell types with infiltration in fewer than 50% of the samples, differential analysis was conducted on 15 immune cell types, revealing six differential immune cell types. Notably, regulatory T cells (Tregs) and M0 macrophages were more highly infiltrated in the high-risk group, whereas activated natural killer (NK) cells, monocytes, resting myeloid dendritic cells, and activated mast cells were more prominent in the low-risk group (Fig. 8b). Correlation analysis demonstrated a strong positive correlation between M0 macrophages and PI3 and SLN, while activated mast cells exhibited a negative correlation with SLN (Fig. 8c). In parallel, 23 differential immune checkpoints were identified, with ADORA2A, HHLA2, and TNFRSF14 showing higher expression in the low-risk group, while the remaining

Table 1 Results of PH assumption test in univariate Cox regression

Gene	chisq	df	*p*
SLC9A4	3.32075667	1	0.068410336
SIX4	3.069225037	1	0.079787499
AQP6	2.894106972	1	0.088904029
HAO1	2.563653396	1	0.109345631
PAGE2	2.268193144	1	0.132053781
MAGEC2	2.158161539	1	0.141814277
SCNN1A	1.755901779	1	0.185136513
CLCNKB	1.383226773	1	0.239552274
CA10	1.085446647	1	0.297482291
SLN	1.082182026	1	0.298209934
CLDN8	1.002831615	1	0.316626309
MMP13	0.996081288	1	0.318260583
NUPR1L	0.948551193	1	0.330088353
SBSN	0.792913303	1	0.373220658
RP11.35N6.1	0.749193753	1	0.386731614
VAT1L	0.713067911	1	0.398427217
REG1B	0.642661061	1	0.422748828
MAGEA3	0.640195852	1	0.423639885
TEX19	0.625422524	1	0.42903935
UMOD	0.48564859	1	0.485874817
KRT6B	0.386051481	1	0.534382248
ITIH1	0.338135512	1	0.560907422
TFCP2L1	0.330223734	1	0.565527375
CWH43	0.321620485	1	0.570635416
MAL	0.285764359	1	0.592947702
RAB25	0.265298747	1	0.606502991
MAGEC3	0.240724066	1	0.623683645
SLC4A1	0.2298466	1	0.631637596
FXYD4	0.218776317	1	0.63997389
MUC17	0.212054766	1	0.645161644
HSD11B2	0.193573884	1	0.659958602
SSX1	0.10568372	1	0.745112711
PI3	0.079754134	1	0.777630877
PCP4	0.05658088	1	0.811983974
AADAC	0.040864701	1	0.839799308
ATP6V0A4	0.023623565	1	0.877846605
GPR110	0.021903707	1	0.88234355
KLK2	0.017008579	1	0.896236564
TMEM213	0.010434236	1	0.918639115
SLC38A3	0.004768222	1	0.944947979
PROX1	0.00227973	1	0.96191826

Results of PH Assumption Test in Univariate Cox Regression Table presents the results of the proportional hazards (PH) assumption test for 137 candidate genes in the univariate Cox regression analysis. It includes the p-values for each gene's PH assumption test, with those passing the assumption ($p > 0.05$) being selected for subsequent analyses. Genes that met the PH assumption criteria were considered for further evaluation in LASSO and multivariate Cox regression to identify potential prognostic biomarkers for ccRCC

20 immune checkpoints were more highly expressed in the high-risk group (Fig. 8d). The relationship between differential immune checkpoints and prognostic genes revealed that SLN and PI3 were positively correlated with a greater number of differential immune checkpoints, while PCP4 exhibited a negative correlation with five of these checkpoints (Fig. 8e). The expression levels of SLN and PI3 may thus influence the efficacy of immune checkpoint inhibitor therapy.

Gene VHL exhibited the highest mutation frequency

Mutation analysis of the top 20 mutated genes in somatic cells revealed that VHL exhibited the highest mutation frequency in both risk groups, with missense mutations being the predominant mutation type (Fig. 9a, b). Using the optimal threshold for TMB scores (1.078947), patients in the training set were stratified into high and low TMB score groups (Fig. 9c), with high TMB scores correlating with significantly lower survival probabilities.

Sensitive drugs were identified in high and low risk groups

Drug sensitivity analysis using the Wilcoxon test revealed that the IC_{50} values of 27 drugs, including AS601245, Epothilone B, FH535, GSK.650,394, and EHT.1864, were significantly higher in the high-risk group (Fig. 10a). Conversely, 63 drugs, such as JNK.Inhibitor.VIII, BX.795, ZM.447,439, RO.3306, and X17.AAG, showed higher IC50 values in the low-risk group (Fig. 10b).

TF-mRNA regulatory network of prognostic genes

In the TF-mRNA regulatory network, 34 TFs were predicted by PROX1, 4 by PCP4, and 3 by VAT1L, with no TFs predicted by SLN, PI3, or KLK2. The network consisted of 43 nodes and 42 edges, with TF RAD21 simultaneously regulating VAT1L and PCP4, and CTCF regulating both VAT1L and PROX1 (Fig. 11).

Discussion

ccRCC is the most prevalent type of kidney cancer and a leading cause of cancer-related mortality(Brannon et al. 2010). Despite the advent of new immunotherapies and tyrosine kinase inhibitors (TKIs), metastasis and mortality rates continue to rise annually. CA frequently accompanies cancer cells, and it has been established as a key factor in the development of various tumors and poor prognosis(Fukasawa 2005; Levine et al. 2017; Zhang et al. 2020). However, the specific molecular mechanisms underlying CARGs and their relationship with ccRCC remain poorly understood. This study identifies six prognostic genes (PCP4, SLN, PI3, PROX1, VAT1L, and KLK2) through comprehensive bioinformatics analysis to address this gap, and constructs

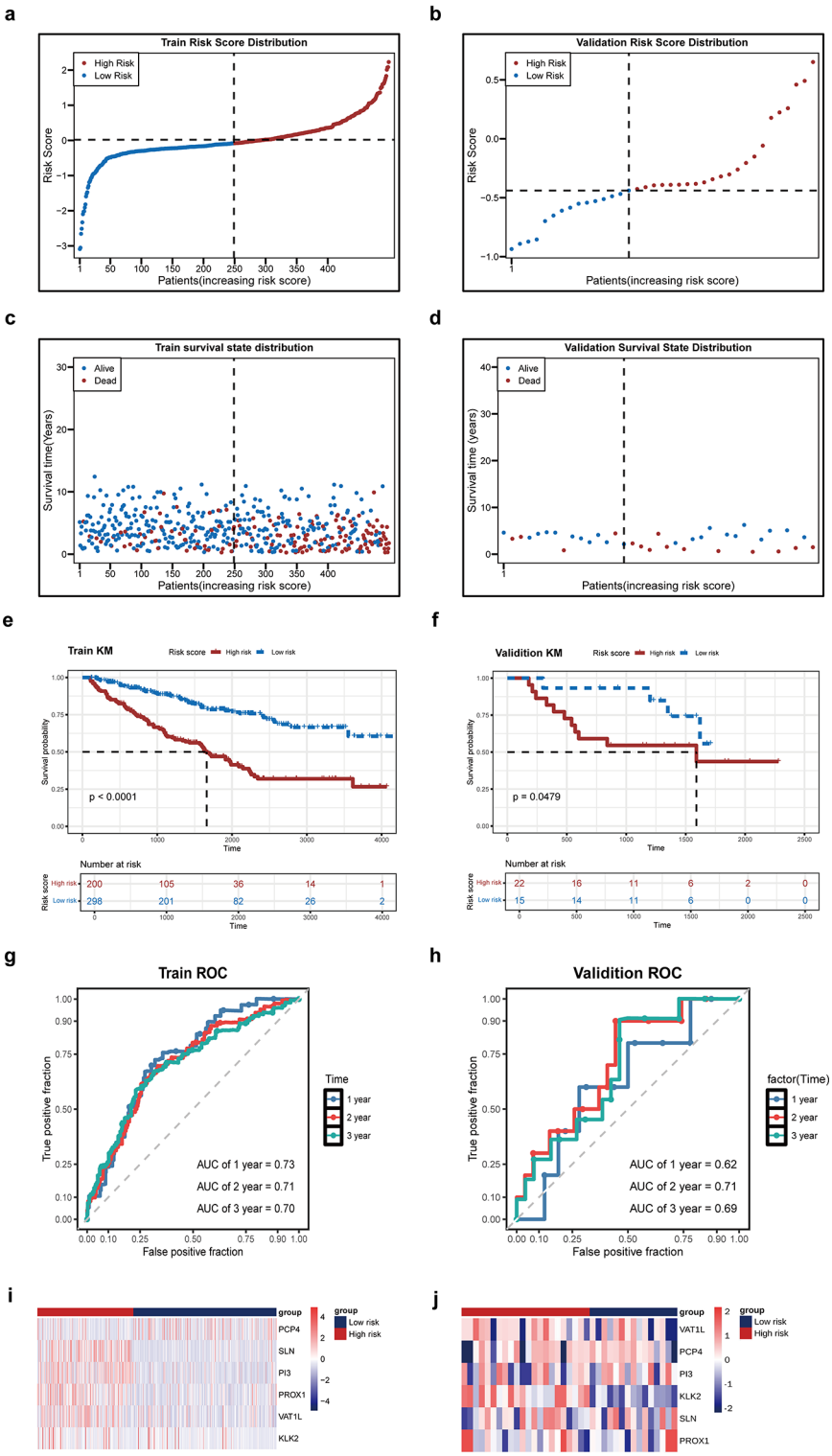

Fig. 4 Validation of the risk model. **a-b** Risk profiles of the training set TCGA-KIRC and validation set GSE29609 samples.**c-d** Survival state distribution of the training set TCGA-KIRC and validation set GSE29609 samples. **e-f** KM curves for high and low risk groups in the training set TCGA-KIRC and validation set GSE29609. **g-h** ROC curves of the model in the training set TCGA-KIRC and the validation set GSE29609. **i-j** Heatmap of prognostic gene expression in high and low risk groups (training set TCGA-KIRC and validation set GSE29609)

and validates a risk model based on these genes. Compared to previous studies that focused on single genes or limited datasets (Imamura and Kiyama 2024; Peng et al. 2022), this study utilizes various public datasets (such as TCGA, ICGC, and GEO), providing a reliable prognostic prediction and personalized treatment guidance. Moreover, past studies that isolated immune and mutation analyses (Fukuda et al. 2016; Song et al. 2024) did not approach the issue from a comprehensive clinical application perspective. In contrast, this study integrates immune microenvironment analysis, mutation patterns, and drug sensitivity data,

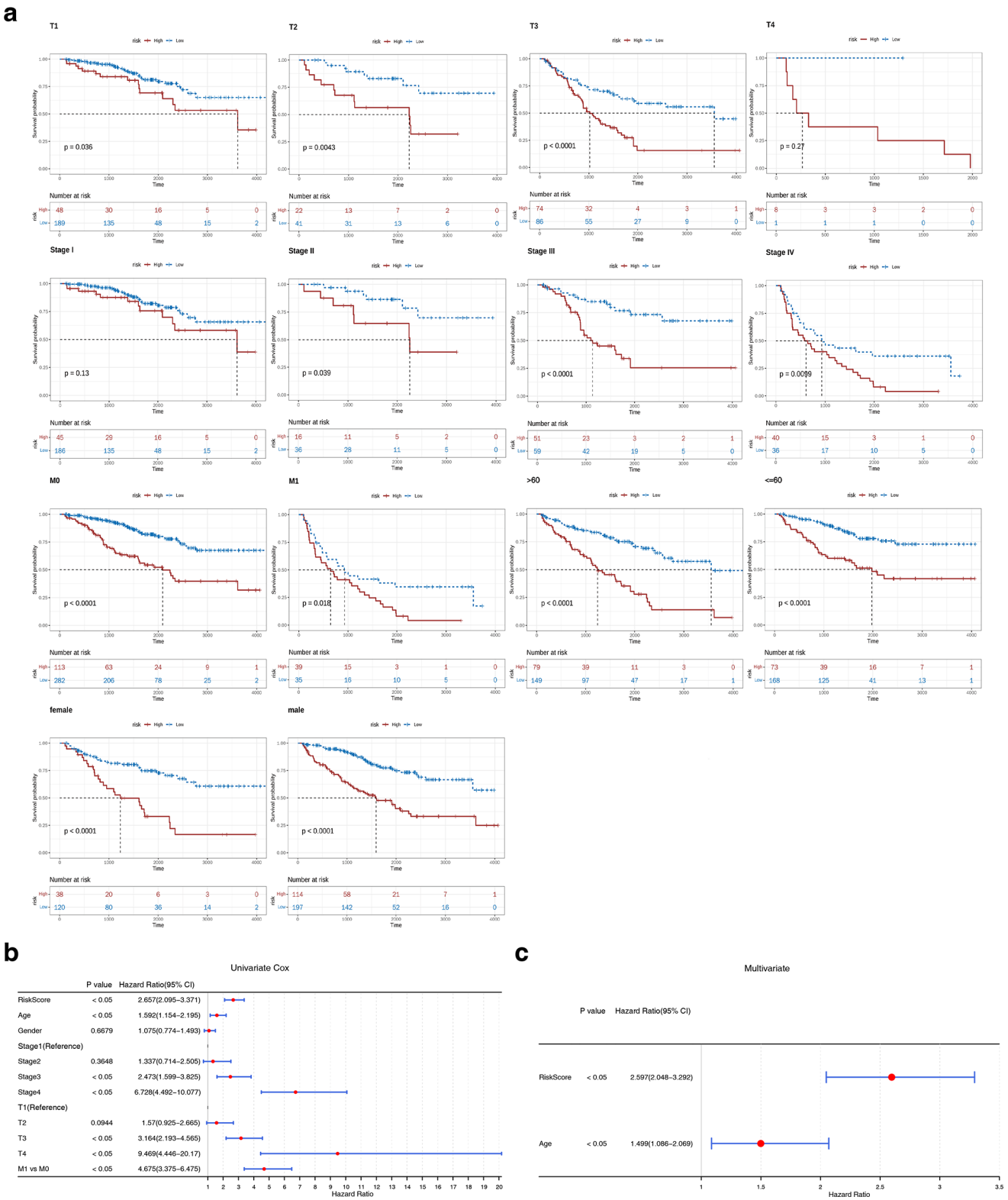

Fig. 5 Screening for independent prognostic factors. **a** Risk score analysis of K-M survival curves for different clinical characteristics. **b** Forest plot of Univariate Cox regression analysis of clinical data information and risk scores for all ccRCC patients in the training set TCGA-KIRC. **c** Multivariate Cox regression screening for independent prognostic factors

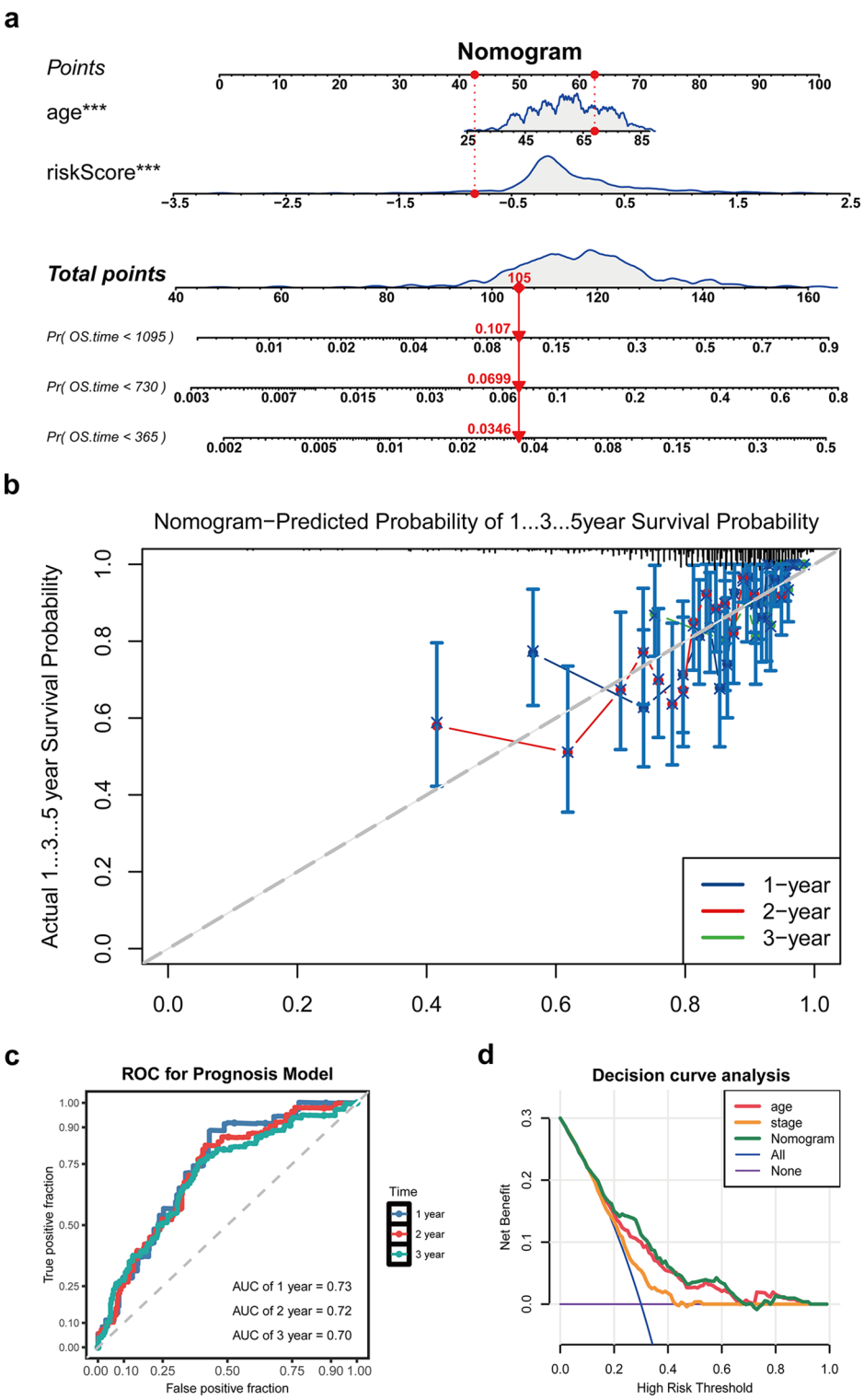

Fig. 6 Nomogram constructed based on independent prognostic factors. **a** Nomogram constructed based on independent prognostic factors. **b** The 1-year, 3-year, and 5-year calibration curves for the nomogram. **c** The 1-year, 3-year, and 5-year ROC curves for the nomogram.**d** The DCA for the nomogram

offering new insights for personalized prognosis and treatment response evaluation that are clinically relevant.

The six prognostic genes identified in this study have substantial clinical and biological significance. KLK2, a serine protease, is well-known for its involvement in prostate cancer (Pca) (Nam et al. 2006; Paniagua-Herranz et al. 2024) and has also been linked to ccRCC (Rae et al. 1999). GSEA reveals that KLK2 is enriched in renal cell carcinoma pathways, further establishing its relevance to ccRCC development. Elevated KLK2 expression correlates with higher tumor grades and stages in Pca, and its fusion with FGFR2 promotes cancer cell growth and metastasis

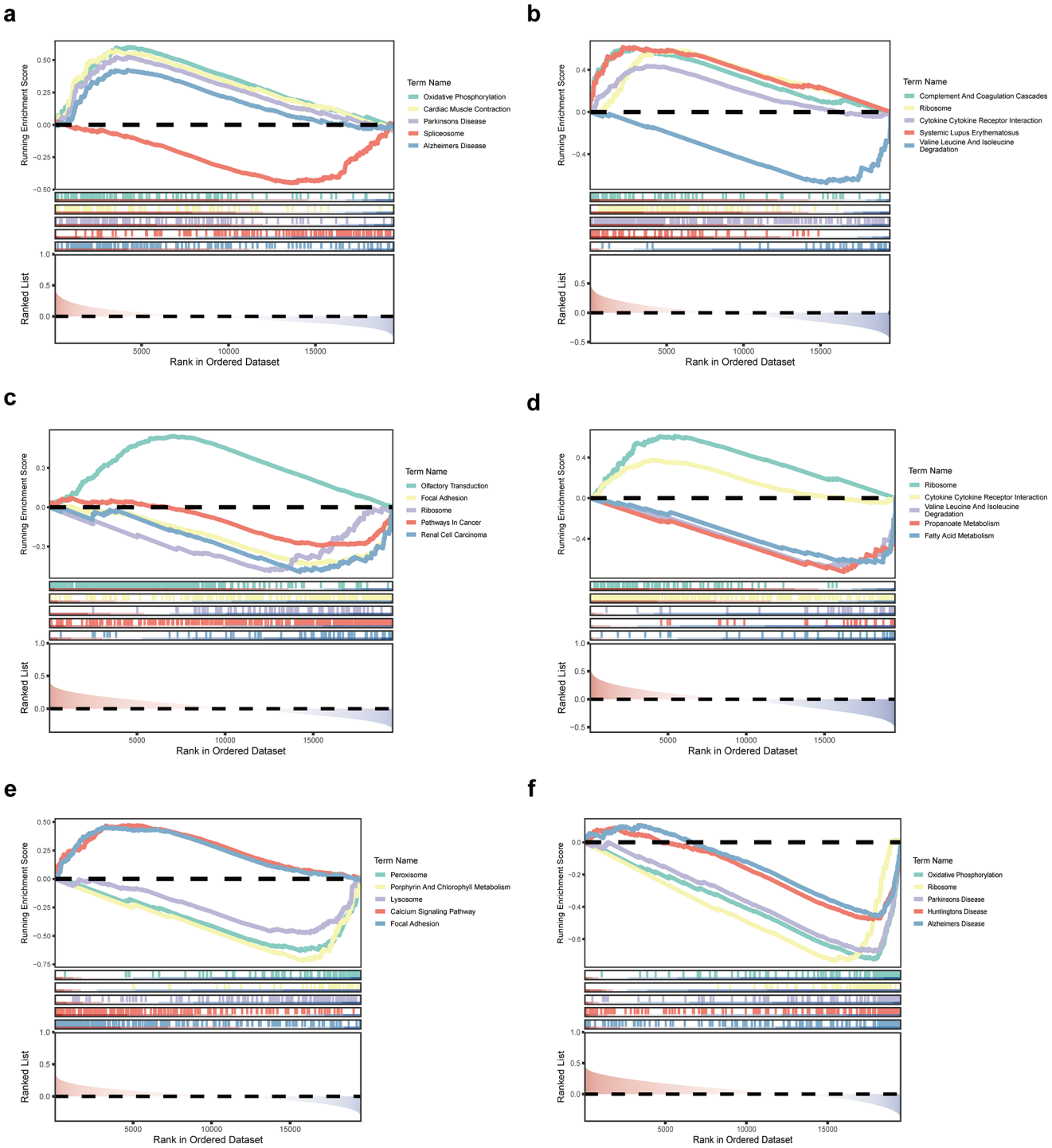

Fig. 7 GSEA based on prognostic genes **a** PCP4, **b** SLN, **c** KLK2, **d** PL3, **e** VAT1L, **f** PROX1

(Krook et al. 2019). Moreover, KLK2 expression is upregulated through promoter demethylation mediated by protein kinase N (PKN), a key regulator of the PI3K pathway involved in cell cycle progression and centrosome function. This epigenetic regulation links KLK2 to PI3K-mediated cell cycle control and centrosome amplification, supporting its role in tumorigenesis(Giles et al. 2021; Metzger et al. 2008; Oikonomopoulou et al. 2010). KLK2's association with the immune microenvironment and its mild correlation with TMPRSS2 deletion suggest a multifaceted role in cancer progression (Nam et al. 2006; Paniagua-Herranz et al. 2024).

PCP4 is the sole protective factor among the six prognostic genes identified in this study. As Purkinje cell protein 4

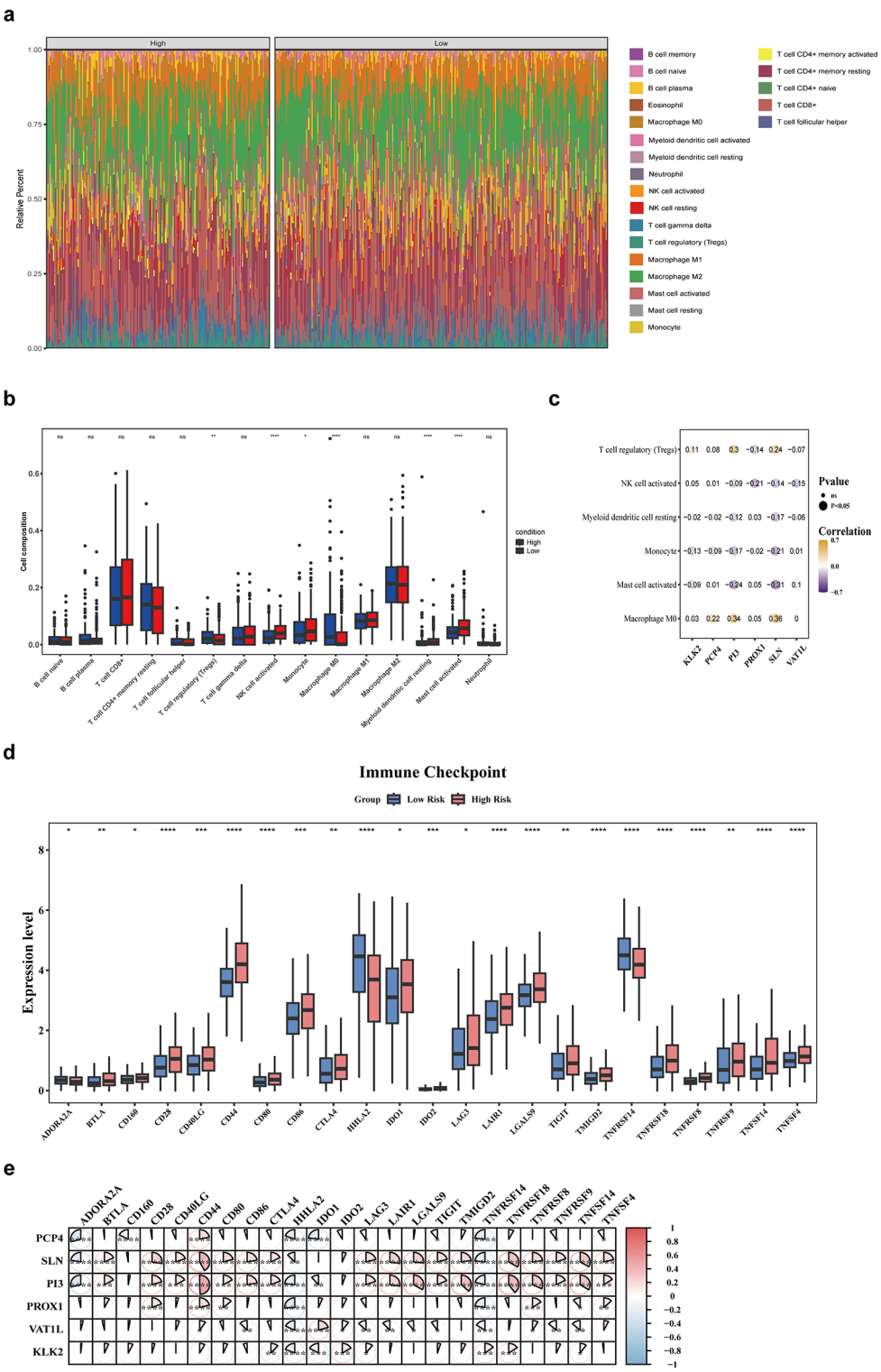

Fig. 8 Immune infiltration and differential immune checkpoint analysis. **a** The xCell algorithm assesses the distribution of immune cells in high and low risk groups. **b** Differences in the distribution of immune cell infiltration between high and low risk groups. **c** Correlation analysis of differential immune cells and prognostic genes between high and low risk groups. **d** Boxplot of difference analysis of common immune checkpoints between groups for high and low risk groups. **e** Correlation of prognostic genes with differential immune checkpoints. ns: not significant, *: $p<0.05$, **: $p<0.01$, ***: $p<0.001$, ****: $p<0.0001$

peptide, it works in conjunction with PEP19 to exert anti-apoptotic effects (Hamada et al. 2014). Research has shown that the PCP4/PEP19 complex not only plays a role in neuronal differentiation but also influences the tumor microenvironment by regulating calcium deposition and mineral nodule formation in osteoblasts (Kitazono et al. 2020). Recent studies highlight PCP4's significant involvement in the regulation of calmodulin, a calcium-binding messenger protein critical for various cellular processes, including apoptosis and cell proliferation. Notably, miR-122 has been found to regulate osteoblast differentiation by targeting PCP4, which in turn inhibits osteoblast proliferation and

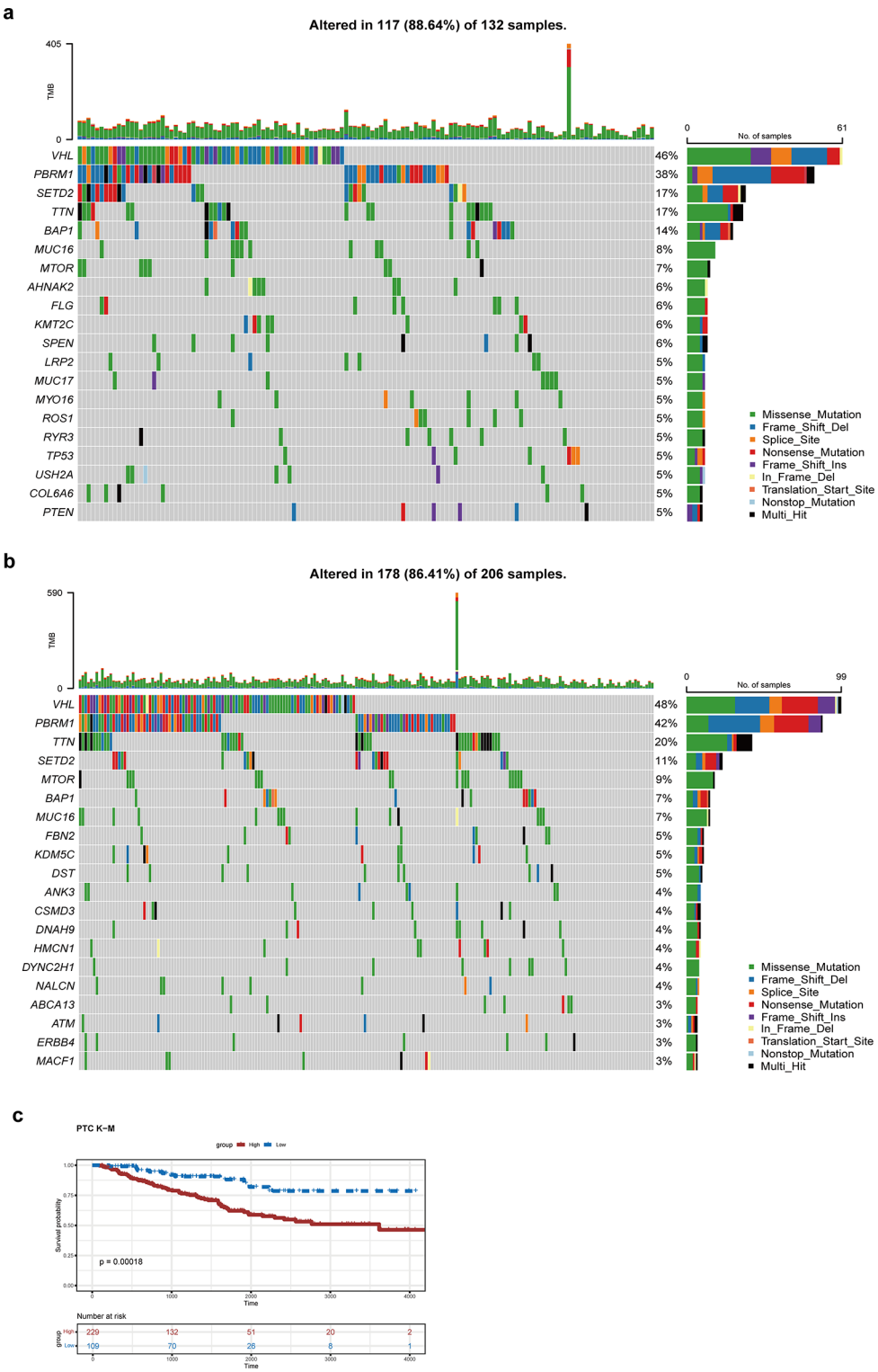

Fig. 9 Mutation analysis based on high and low risk groups. **a** Waterfall plot of tumour somatic cell mutations in the high risk group. **b** Waterfall plot of tumour somatic mutations in the low risk group. **c** Survival differences in TMB scores between high and low risk groups

differentiation through activation of the JNK pathway(Meng et al. 2020). Moreover, alterations in PCP4 expression have been linked to changes in centrosome dynamics, which contribute to CA, a hallmark of cancer cells. This suggests that PCP4 may regulate centrosome stability in addition to its role in promoting cell survival. Knockdown of PCP4 expression *via* siRNA results in significant increases in neuronal outgrowth and centrosome fragmentation, underscoring its critical role in both centrosome integrity and the cell cycle(Kitazono et al. 2020; Paniagua-Herranz et al. 2024; Venables et al. 1988). The anti-apoptotic functions of PCP4/PEP19 have also been observed in breast cancer cell

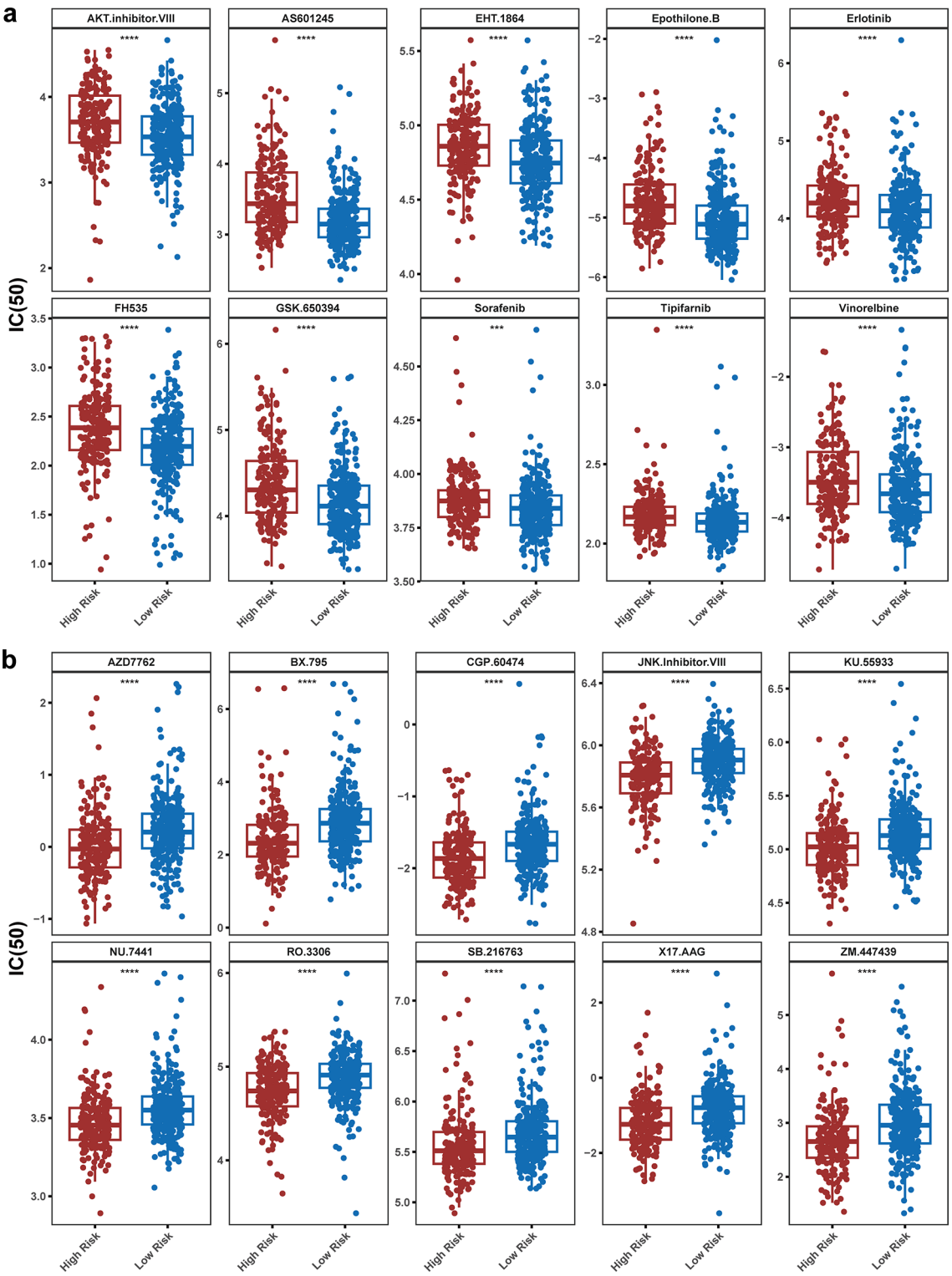

Fig. 10 Drug sensitivity analysis **a-b** Differences in IC50 of drugs between high and low risk groups. ***: $p<0.001$, ****: $p<0.0001$

lines, where it inhibits apoptosis and promotes cell survival through modulation of the Akt and JNK pathways(Hamada et al. 2014; Yoshimura et al. 2016). These findings highlight the multifaceted roles of PCP4 in ccRCC progression, including its impact on cell proliferation, apoptosis, centrosome amplification, and overall tumorigenesis.

PI3 kinase is a central mediator in immune cell signaling networks, playing an essential role in immune cell

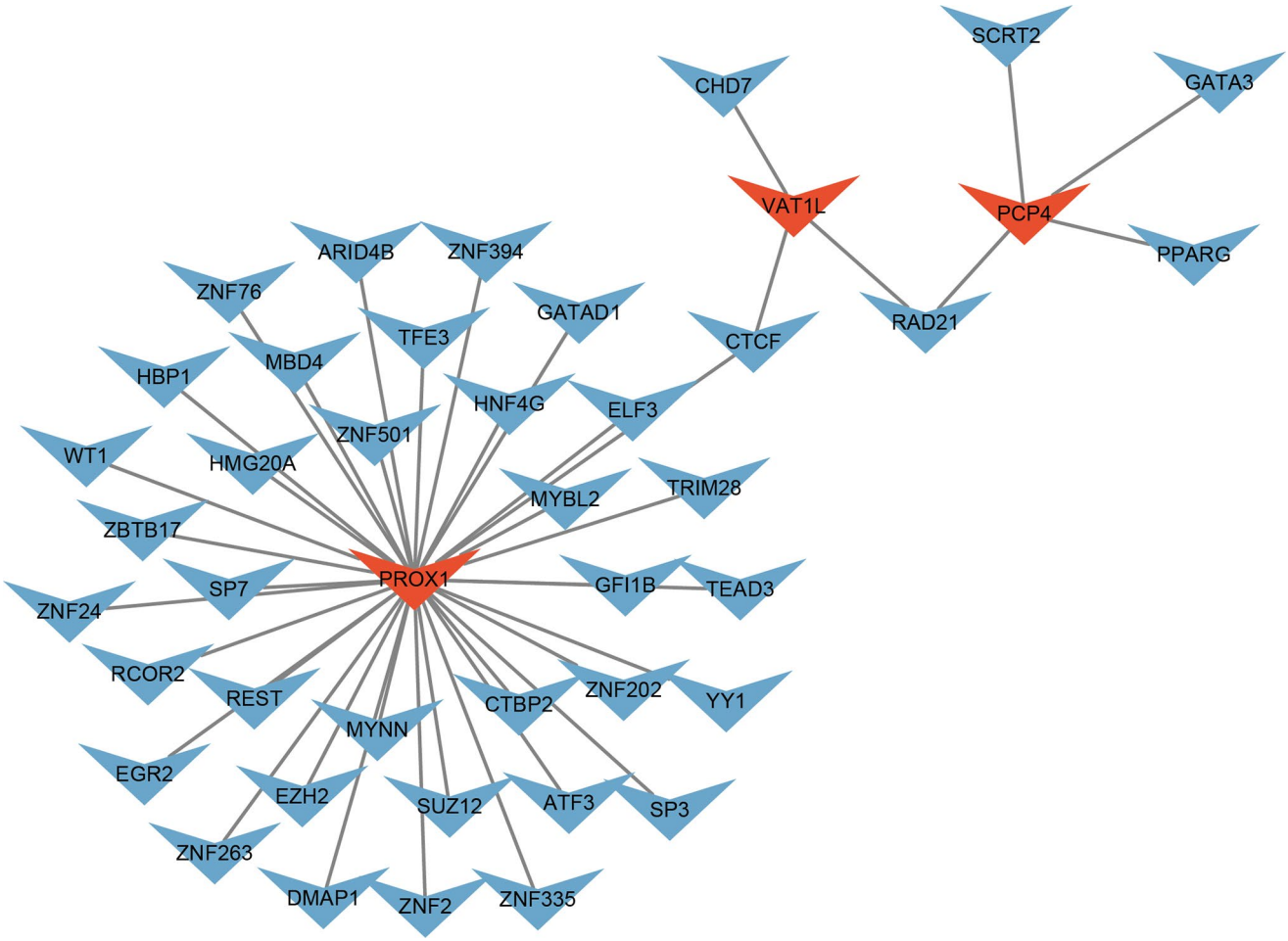

Fig. 11 TF regulatory network of prognostic genes. Prognostic markers in red and TF in blue

differentiation, proliferation, and survival (Leisching 2019). As a second messenger, PI3K is particularly critical for T cell function, notably in regulating the development and survival of Th cell subpopulations (Stegeman et al. 2014). Recent studies have revealed that PI3K pathway activation is also implicated in CA. For example, oncogenic mutations in PIK3CA, which activate the PI3K-AKT signaling pathway, have been shown to induce centrosome amplification. This process involves downstream effectors such as AKT, ROCK, and CDK2/Cyclin E-nucleophosmin, and contributes to increased cellular tolerance to genome doubling (Berenjeno et al. 2017). Additionally, the PI3K-Akt pathway is implicated in inducing centrosome abnormalities in various cancers, contributing to chromosomal instability and further promoting tumorigenesis (Nam et al. 2010). Studies have shown that elevated PI3K activity is associated with the onset of several immune-related diseases, offering potential targets for therapeutic intervention in the immune microenvironment of patients with ccRCC (Leisching 2019; Nieuwenhuis and Eva 2022; Stegeman et al. 2014).

PROX1 plays a critical role in lymphangiogenesis and exhibits dual functions in various tumors. Elevated PROX1 expression correlates with an undifferentiated tumor cell phenotype, increased lymphatic metastasis, and CA (Wang et al. 2022; Zhu et al. 2022). CA, which enhances tumor cell proliferation and invasion, may be regulated by PROX1 through mechanisms impacting cell cycle progression and centrosomal stability. In ccRCC, while PROX1 expression is lower compared to normal tissue, its overexpression significantly associates with poor prognosis, positioning it as a potential prognostic marker and a contributing factor to CA and tumor aggressiveness (Ho et al. 2023). Furthermore, PROX1 has been implicated in various signaling pathways governing cell proliferation and differentiation. Recent findings highlight its regulation by microRNAs, such as miR-140-5p, which modulate its expression and potentially its role in CA(Ding et al. 2021).

Sarcoplasmic reticulum Ca^{2+}-binding protein (SLN), less studied in the cancer context, has been primarily investigated for its metabolic functions in myocytes, particularly in ATP/Ca^{2+} regulation (Mengeste et al. 2022; Montigny et al. 2021).

SLN maintains calcium homeostasis by regulating sarcoplasmic reticulum Ca^{2+}-ATPase (SERCA1), which is essential for intracellular calcium regulation (Odermatt et al. 1998). Dysregulated calcium signaling, potentially influenced by SLN, is associated with various cellular processes, including microtubule organization and centrosome segregation (Naik and Naik 2011). Disruption of these processes is linked to CA, a hallmark of many cancers, including ccRCC. However, the direct role of SLN in cancer remains underexplored, and the precise relationship between SLN-mediated calcium dysregulation and CA in ccRCC remains unclear.

Although research on VAT1L is limited, existing studies highlight its prognostic significance in various cancers(Gao et al. 2023). In breast cancer and retinal ganglion cells, VAT1L has been integrated into prognostic models, indicating its potential importance in tumor progression (Huang et al. 2022).

Enrichment analysis reveals that four prognostic genes are co-enriched in ribosomal pathways, closely associated with the invasive characteristics of ccRCC. Nucleolar abnormalities, including changes in the size and shape of the ribosome, are linked to tumor progression in ccRCC. As early as 1982, Fuhrman et al.(Fuhrman et al. 1982) proposed a grading system for RCC tumors based on these and other nuclear parameters, which could predict distant metastasis following nephrectomy, underscoring the connection between ccRCC pathology and nucleolar dysfunction. The nucleolus, a key regulator of cellular function and metabolism, serves as an active site for various non-coding RNAs, including snoRNA, IGS RNA, and miRNA(Tollervey and Kiss 1997). Dysregulation of the nucleolus in ccRCC has been linked to alterations in signaling pathways related to cell survival and proliferation(Yang et al. 2020). Non-coding RNAs, particularly snoRNAs due to their diverse functions, have garnered attention; as miRNA sponges, snoRNAs can regulate miRNA binding to complementary sequences, thereby inhibiting downstream functional expression(Chen et al. 2019b). Additionally, snoRNAs modulate the activity of key transcription factors, leading to transcriptional reprogramming of genes involved in cancer progression(Xu et al. 2020). Recently, the role of nucleolar non-coding RNAs in ccRCC has attracted increasing attention (Popławski et al. 2021) (Furuya et al. 2011), further suggesting that the six prognostic genes may impact the onset and progression of ccRCC *via* ribosomal pathways.

Beyond non-coding RNAs, emerging research indicates that coding long non-coding RNAs (lncRNAs) also play significant roles in cancer, with some capable of protein translation under specific conditions. The CodLncScape framework, which includes codLncDB and codLncFlow, aids in exploring their roles in ccRCC, particularly in ribosomal and nucleolar functions, highlighting potential biomarkers and therapeutic targets (Liu et al. 2024b).

Correlation analysis between immune cells and prognostic genes revealed a strong positive correlation between M0 macrophages and PI3 and SLN, while activated mast cells exhibited a strong negative correlation with SLN. M0 macrophages can polarize into pro-inflammatory (M1) or anti-inflammatory (M2) subtypes in response to various microenvironmental cues, playing a pivotal role in the tumor microenvironment(Xia et al. 2023). In ccRCC, the tumor immune microenvironment (TIME) characterization indicates that patients with high M0 macrophage infiltration tend to have a poor prognosis and exhibit a lower predicted response to immune checkpoint blockade (ICB) therapy. This suggests that PI3 and SLN may influence the progression of ccRCC through their interaction with M0 macrophages. Activated mast cells, which are triggered by antigens or other stimuli, release histamine, cytokines, and bioactive molecules involved in allergic responses and immune regulation(DeBruin et al. 2015). In ccRCC, studies have shown that activated mast cells correlate with poor prognosis, and their enrichment is associated with a reduced response to immunotherapy(Chu et al. 2023). This suggests that mast cells may suppress anti-tumor immunity, thereby contributing to tumor progression. In conclusion, SLN likely influences ccRCC development by modulating the activity of activated mast cells within the tumor immune microenvironment.

Drug sensitivity analysis revealed that the IC_{50} of AS601245 was significantly higher in high-risk patients with ccRCC, while JNK Inhibitor VIII showed a marked downregulation trend in the same cohort. AS601245 is a selective JNK inhibitor that targets the c-Jun N-terminal kinase (JNK) signaling pathway, which regulates critical biological processes such as cell proliferation, apoptosis, and differentiation(Cerbone et al. 2012). In ccRCC, AS601245 modulates tumor cell growth and apoptosis *via* the JNK pathway, potentially contributing to poorer prognosis in high-risk patients(Bai et al. 2022). JNK Inhibitor VIII, another JNK inhibitor, suppresses JNK kinase activity, disrupting cellular stress responses and apoptotic signaling(Zhang et al. 2023b). Research suggests that the downregulation of JNK Inhibitor VIII in ccRCC may help slow tumor progression(Bai et al. 2022). Together, AS601245 and JNK Inhibitor VIII modulate ccRCC biology through the JNK pathway, with AS601245 potentially promoting tumor progression in high-risk patients, while JNK Inhibitor VIII demonstrates tumor-suppressive potential *via* JNK inhibition.

Conclusions

This study identifies six prognostic genes (PCP4, SLN, PI3, PROX1, VAT1L, and KLK2) associated with centrosome amplification in ccRCC and develops a prognostic risk model for patient prediction. The findings underscore the

clinical significance of these genes in ccRCC progression, prognosis, and the tumor immune microenvironment. The proposed model establishes a foundation for personalized treatment strategies and clinical management. Furthermore, this research paves the way for future studies on the roles of CARGs in tumorigenesis, immune modulation, drug sensitivity, and mutational profiling, which should be further validated in clinical settings.

Supplementary Information The online version contains supplementary material available at https://doi.org/10.1007/s00438-025-02237-7.

Acknowledgements We would like to express our sincere gratitude to all individuals and organizations who supported and assisted us throughout this research. We would like to express our sincere gratitude to all individuals and organizations who supported and assisted us throughout this research. Special thanks to the following authors: Wenzhe Ma and Rongyang Dai. In conclusion, we extend our thanks to everyone who has supported and assisted us along the way. Without your support, this research would not have been possible.

Author contributions Conceptualization, B. Z. and Y. W.; methodology, J. H. and L. T.; software, F. L. and Z. Y.; validation, B. Z. and L. T.; formal analysis, B. Z., F. L. and Y. W.; investigation, L. L. Z. Y. and J. H.; resources, B. Z. and Z. Y.; data curation, B. Z. F. L. and L. L.; writing—original draft preparation, B. Z. and Y.W.; writing—review and editing, B. Z. and R. D.; visualization, B. Z. and Y. W.; supervision, R. D. and W. M.; project administration, R. D. and W. M.; funding acquisition, B. Z. R. D. and W. M. All authors have read and agreed to the published version of the manuscript.

Funding This study were funded by the Science and Technology Development Fund, Macau SAR (File no. 0105/2022/A2 and 006/2023/SKL) and Sichuan Science and Technology Program 2022YFS0614 (Y.W.) and Luzhou Science and Technology Program 2024JYJ010 (B.Z.)

Data availability https://portal.gdc.cancer.gov/ TCGA. The datasets used and / or analysed in the current study are available from the corresponding author on reasonable request.

Declarations

Ethical approval Not applicable.

Consent to participate Not applicable.

Consent to publish Not applicable.

Competing interests The authors declare that the study was conducted in the absence of any commercial or financial relationship that could be viewed as a potential conflict of interest.

Open Access This article is licensed under a Creative Commons Attribution-NonCommercial-NoDerivatives 4.0 International License, which permits any non-commercial use, sharing, distribution and reproduction in any medium or format, as long as you give appropriate credit to the original author(s) and the source, provide a link to the Creative Commons licence, and indicate if you modified the licensed material. You do not have permission under this licence to share adapted material derived from this article or parts of it. The images or other third party material in this article are included in the article's Creative Commons licence, unless indicated otherwise in a credit line to the material. If material is not included in the article's Creative Commons licence and your intended use is not permitted by statutory regulation or exceeds the permitted use, you will need to obtain permission directly from the copyright holder. To view a copy of this licence, visit http://creativecommons.org/licenses/by-nc-nd/4.0/.

References

Anderhub SJ, Krämer A, Maier B (2012) Centrosome amplification in tumorigenesis. Cancer Lett 322(1):8–17. https://doi.org/10.1016/j.canlet.2012.02.006

Bai Z, Lu J, Chen A, Zheng X, Wu M, Tan Z, Xie J (2022) Identification and Validation of Cuproptosis-Related LncRNA Signatures in the Prognosis and Immunotherapy of Clear Cell Renal Cell Carcinoma Using Machine Learning. Biomolecules 12(12). https://doi.org/10.3390/biom12121890

Berenjeno IM, Piñeiro R, Castillo SD, Pearce W, McGranahan N, Dewhurst SM, Meniel V, Birkbak NJ, Lau E, Sansregret L, Morelli D, Kanu N, Srinivas S, Graupera M, Parker VER, Montgomery KG, Moniz LS, Scudamore CL, Phillips WA, Semple RK, Clarke A, Swanton C, Vanhaesebroeck B (2017) Oncogenic PIK3CA induces centrosome amplification and tolerance to genome doubling. Nat Commun 8(1):1773. https://doi.org/10.1038/s41467-017-02002-4

Bose A, Dalal SN (2019) Centrosome amplification and tumorigenesis: cause or effect?? Results Probl Cell Differ 67:413–440. https://doi.org/10.1007/978-3-030-23173-6_18

Brannon AR, Reddy A, Seiler M, Arreola A, Moore DT, Pruthi RS, Wallen EM, Nielsen ME, Liu H, Nathanson KL, Ljungberg B, Zhao H, Brooks JD, Ganesan S, Bhanot G, Rathmell WK (2010) Molecular stratification of clear cell renal cell carcinoma by consensus clustering reveals distinct subtypes and survival patterns. Genes Cancer 1(2):152–163. https://doi.org/10.1177/1947601909359929

Cerbone A, Toaldo C, Pizzimenti S, Pettazzoni P, Dianzani C, Minelli R, Ciamporcero E, Roma G, Dianzani MU, Canaparo R, Ferretti C, Barrera G (2012) AS601245, an Anti-Inflammatory JNK inhibitor, and Clofibrate have a synergistic effect in inducing cell responses and in affecting the gene expression profile in CaCo-2 Colon cancer cells. PPAR Res 2012(269751). https://doi.org/10.1155/2012/269751

Chen F, Yang Y, Zhao Y, Pei L, Yan H (2019a) Immune infiltration profiling in nonsmall cell lung Cancer and their clinical significance: study based on gene expression measurements. DNA Cell Biol 38(11):1387–1401. https://doi.org/10.1089/dna.2019.4899

Chen Q, Zhou W, Du SQ, Gong DX, Li J, Bi JB, Li ZH, Zhang Z, Li ZL, Liu XK, Kong CZ (2019b) Overexpression of SNHG12 regulates the viability and invasion of renal cell carcinoma cells through modulation of HIF1α. Cancer Cell Int 19:128. https://doi.org/10.1186/s12935-019-0782-5

Chu J, Liu W, Hu X, Zhang H, Jiang J (2023) P2RY13 is a prognostic biomarker and associated with immune infiltrates in renal clear cell carcinoma: A comprehensive bioinformatic study. Health Sci Rep 6(12):e1646. https://doi.org/10.1002/hsr2.1646

DeBruin EJ, Gold M, Lo BC, Snyder K, Cait A, Lasic N, Lopez M, McNagny KM, Hughes MR (2015) Mast cells in human health and disease. Methods Mol Biol 1220:93–119. https://doi.org/10.1007/978-1-4939-1568-2_7

Denu RA, Zasadil LM, Kanugh C, Laffin J, Weaver BA, Burkard ME (2016) Centrosome amplification induces high grade features and

is prognostic of worse outcomes in breast cancer. BMC Cancer 16:47. https://doi.org/10.1186/s12885-016-2083-x

Ding K, Lai Z, Yang G, Zeng L (2021) MiR-140-5p targets Prox1 to regulate the proliferation and differentiation of neural stem cells through the ERK/MAPK signaling pathway. Ann Transl Med 9(8):671. https://doi.org/10.21037/atm-21-597

Ding G, Wang T, Tang G, Zou Q, Wu G, Wu J (2024) A novel prognostic predictor of immune microenvironment and therapeutic response in clear cell renal cell carcinoma based on angiogenesis-immune-related gene signature. Heliyon 10(1):e23503. https://doi.org/10.1016/j.heliyon.2023.e23503

Friedman J, Hastie T, Tibshirani R (2010) Regularization paths for generalized linear models via coordinate descent. J Stat Softw 33(1):1–22

Fuhrman SA, Lasky LC, Limas C (1982) Prognostic significance of morphologic parameters in renal cell carcinoma. Am J Surg Pathol 6(7):655–663. https://doi.org/10.1097/00000478-198210000-00007

Fukasawa K (2005) Centrosome amplification, chromosome instability and cancer development. Cancer Lett 230(1):6–19. https://doi.org/10.1016/j.canlet.2004.12.028

Fukuda T, Tsuruga T, Kuroda T, Nishikawa H, Ohta T (2016) Functional link between BRCA1 and BAP1 through histone H2A, heterochromatin and DNA damage response. Curr Cancer Drug Targets 16(2):101–109. https://doi.org/10.2174/1568009615666151030102427

Furuya N, Kamai T, Shirataki H, Yanai Y, Fukuda T, Mizuno T, Nakamura F, Kambara T, Nakanishi K, Abe H, Yoshida K (2011) Serum interferon alpha receptor 2 mRNA May predict efficacy of interferon alpha with/without low-dose Sorafenib for metastatic clear cell renal cell carcinoma. Cancer Immunol Immunother 60(6):793–808. https://doi.org/10.1007/s00262-011-0989-3

Gao ZJ, Fang Z, Yuan JP, Sun SR, Li B (2023) Integrative multi-omics analyses unravel the immunological implication and prognostic significance of CXCL12 in breast cancer. Front Immunol 14:1188351. https://doi.org/10.3389/fimmu.2023.1188351

Gao CH, Chen C, Akyol T, Dusa A, Yu G, Cao B, Cai P (2024) GgVennDiagram: intuitive Venn diagram software extended. Imeta 3(1):e177. https://doi.org/10.1002/imt2.177

Giles KA, Gould CM, Achinger-Kawecka J, Page SG, Kafer GR, Rogers S, Luu PL, Cesare AJ, Clark SJ, Taberlay PC (2021) BRG1 knockdown inhibits proliferation through multiple cellular pathways in prostate cancer. Clin Epigenetics 13(1):37. https://doi.org/10.1186/s13148-021-01023-7

Godinho SA, Picone R, Burute M, Dagher R, Su Y, Leung CT, Polyak K, Brugge JS, Théry M, Pellman D (2014) Oncogene-like induction of cellular invasion from centrosome amplification. Nature 510(7503):167–171. https://doi.org/10.1038/nature13277

Gu Z (2022) Complex heatmap visualization. Imeta 1(3):e43. https://doi.org/10.1002/imt2.43

Hamada T, Souda M, Yoshimura T, Sasaguri S, Hatanaka K, Tasaki T, Yoshioka T, Ohi Y, Yamada S, Tsutsui M, Umekita Y, Tanimoto A (2014) Anti-apoptotic effects of PCP4/PEP19 in human breast cancer cell lines: a novel oncotarget. Oncotarget 5(15):6076–6086. https://doi.org/10.18632/oncotarget.2161

Ho YC, Geng X, O'Donnell A, Ibarrola J, Fernandez-Celis A, Varshney R, Subramani K, Azartash-Namin ZJ, Kim J, Silasi R, Wylie-Sears J, Alvandi Z, Chen L, Cha B, Chen H, Xia L, Zhou B, Lupu F, Burkhart HM, Aikawa E, Olson LE, Ahamed J, López-Andrés N, Bischoff J, Yutzey KE, Srinivasan RS (2023) PROX1 inhibits PDGF-B expression to prevent myxomatous degeneration of heart valves. Circ Res 133(6):463–480. https://doi.org/10.1161/circresaha.123.323027

Hu FF, Liu CJ, Liu LL, Zhang Q, Guo AY (2021) Expression profile of immune checkpoint genes and their roles in predicting immunotherapy response. Brief Bioinform 22(3). https://doi.org/10.1093/bib/bbaa176

Huang W, Xu Q, Su J, Tang L, Hao ZZ, Xu C, Liu R, Shen Y, Sang X, Xu N, Tie X, Miao Z, Liu X, Xu Y, Liu F, Liu Y, Liu S (2022) Linking transcriptomes with morphological and functional phenotypes in mammalian retinal ganglion cells. Cell Rep 40(11):111322. https://doi.org/10.1016/j.celrep.2022.111322

Imamura I, Kiyama R (2024) Potential involvement of KANK1 haploinsufficiency in centrosome aberrations. Biochim Biophys Acta Gen Subj 1868(8):130648. https://doi.org/10.1016/j.bbagen.2024.130648

Jiang H, Li Y, Wang T (2021) Comparison of Billroth I, Billroth II, and Roux-en-Y reconstructions following distal gastrectomy: A systematic review and network meta-analysis. Cir Esp (Engl Ed) 99(6):412–420. https://doi.org/10.1016/j.cireng.2020.09.018

Kasyanov ED, Yakovleva YV, Mudrakova TA, Kasyanova AA, Mazo GE (2023) Comorbidity patterns and structure of depressive episodes in patients with bipolar disorder and major depressive disorder. Zh Nevrol Psikhiatr Im S S Korsakova 123(11 Vyp 2):108–114. https://doi.org/10.17116/jnevro2023123112108

Kitazono I, Hamada T, Yoshimura T, Kirishima M, Yokoyama S, Akahane T, Tanimoto A (2020) PCP4/PEP19 downregulates neurite outgrowth via transcriptional regulation of Ascl1 and NeuroD1 expression in human neuroblastoma M17 cells. Lab Invest 100(12):1551–1563. https://doi.org/10.1038/s41374-020-0462-z

Krook MA, Barker H, Chen HZ, Reeser JW, Wing MR, Martin D, Smith AM, Dao T, Bonneville R, Samorodnitsky E, Miya J, Freud AG, Monk JP, Clinton SK, Roychowdhury S (2019) Characterization of a KLK2-FGFR2 fusion gene in two cases of metastatic prostate cancer. Prostate Cancer Prostatic Dis 22(4):624–632. https://doi.org/10.1038/s41391-019-0145-2

Leisching GR (2019) PI3-Kinase Δγ catalytic isoforms regulate the Th-17 response in tuberculosis. Front Immunol 10:2583. https://doi.org/10.3389/fimmu.2019.02583

Levine MS, Bakker B, Boeckx B, Moyett J, Lu J, Vitre B, Spierings DC, Lansdorp PM, Cleveland DW, Lambrechts D, Foijer F, Holland AJ (2017) Centrosome amplification is sufficient to promote spontaneous tumorigenesis in mammals. Dev Cell 40(3):313–322e315. https://doi.org/10.1016/j.devcel.2016.12.022

Liu TT, Li R, Huo C, Li JP, Yao J, Ji XL, Qu YQ (2021) Identification of CDK2-Related immune forecast model and CeRNA in lung adenocarcinoma, a Pan-Cancer analysis. Front Cell Dev Biol 9:682002. https://doi.org/10.3389/fcell.2021.682002

Liu C, He Y, Luo J (2024a) Application of chest CT imaging feature model in distinguishing squamous cell carcinoma and adenocarcinoma of the lung. Cancer Manag Res 16:547–557. https://doi.org/10.2147/cmar.S462951

Liu T, Qiao H, Wang Z, Yang X, Pan X, Yang Y, Ye X, Sakurai T, Lin H, Zhang Y (2024b) CodLncScape provides a Self-Enriching framework for the systematic collection and exploration of coding LncRNAs. Adv Sci (Weinh) 11(22):e2400009. https://doi.org/10.1002/advs.202400009

Liu Y, He M, Ke X, Chen Y, Zhu J, Tan Z, Chen J (2024c) Centrosome amplification-related signature correlated with immune microenvironment and treatment response predicts prognosis and improves diagnosis of hepatocellular carcinoma by integrating machine learning and single-cell analyses. Hepatol Int 18(1):108–130. https://doi.org/10.1007/s12072-023-10538-5

Love MI, Huber W, Anders S (2014) Moderated Estimation of fold change and dispersion for RNA-seq data with DESeq2. Genome Biol 15(12):550. https://doi.org/10.1186/s13059-014-0550-8

Makhov P, Joshi S, Ghatalia P, Kutikov A, Uzzo RG, Kolenko VM (2018) Resistance to systemic therapies in clear cell renal cell carcinoma: mechanisms and management strategies. Mol Cancer Ther 17(7):1355–1364. https://doi.org/10.1158/1535-7163.Mct-17-1299

Meng YC, Lin T, Jiang H, Zhang Z, Shu L, Yin J, Ma X, Wang C, Gao R, Zhou XH (2020) miR-122 exerts inhibitory effects on osteoblast proliferation/differentiation in osteoporosis by activating the PCP4-Mediated JNK pathway. Mol Ther Nucleic Acids 20:345–358. https://doi.org/10.1016/j.omtn.2019.11.038

Mengeste AM, Katare P, Dalmao Fernandez A, Lund J, Bakke HG, Baker D, Bartesaghi S, Peng XR, Rustan AC, Thoresen GH, Kase ET (2022) Knockdown of Sarcolipin (SLN) impairs substrate utilization in human skeletal muscle cells. Mol Biol Rep 49(7):6005–6017. https://doi.org/10.1007/s11033-022-07387-0

Metzger E, Yin N, Wissmann M, Kunowska N, Fischer K, Friedrichs N, Patnaik D, Higgins JM, Potier N, Scheidtmann KH, Buettner R, Schüle R (2008) Phosphorylation of histone H3 at threonine 11 establishes a novel chromatin mark for transcriptional regulation. Nat Cell Biol 10(1):53–60. https://doi.org/10.1038/ncb1668

Mittal K, Kaur J, Jaczko M, Wei G, Toss MS, Rakha EA, Janssen EAM, Søiland H, Kucuk O, Reid MD, Gupta MV, Aneja R (2021) Centrosome amplification: a quantifiable cancer cell trait with prognostic value in solid malignancies. Cancer Metastasis Rev 40(1):319–339. https://doi.org/10.1007/s10555-020-09937-z

Montigny C, Huang DL, Beswick V, Barbot T, Jaxel C, le Maire M, Zheng JS, Jamin N (2021) Sarcolipin alters SERCA1a interdomain communication by impairing binding of both calcium and ATP. Sci Rep 11(1):1641. https://doi.org/10.1038/s41598-021-81061-6

Muglia VF, Prando A (2015) Renal cell carcinoma: histological classification and correlation with imaging findings. Radiol Bras 48(3):166–174. https://doi.org/10.1590/0100-3984.2013.1927

Naik MU, Naik UP (2011) Calcium- and integrin-binding protein 1 regulates microtubule organization and centrosome segregation through Polo like kinase 3 during cell cycle progression. Int J Biochem Cell Biol 43(1):120–129. https://doi.org/10.1016/j.biocel.2010.10.003

Nam RK, Zhang WW, Klotz LH, Trachtenberg J, Jewett MA, Sweet J, Toi A, Teahan S, Venkateswaran V, Sugar L, Loblaw A, Siminovitch K, Narod SA (2006) Variants of the hK2 protein gene (KLK2) are associated with serum hK2 levels and predict the presence of prostate cancer at biopsy. Clin Cancer Res 12(21):6452–6458. https://doi.org/10.1158/1078-0432.Ccr-06-1485

Nam HJ, Chae S, Jang SH, Cho H, Lee JH (2010) The PI3K-Akt mediates oncogenic Met-induced centrosome amplification and chromosome instability. Carcinogenesis 31(9):1531–1540. https://doi.org/10.1093/carcin/bgq133

Nieuwenhuis B, Eva R (2022) Promoting axon regeneration in the central nervous system by increasing PI3-kinase signaling. Neural Regen Res 17(6):1172–1182. https://doi.org/10.4103/1673-5374.327324

Noone AM, Cronin KA, Altekruse SF, Howlader N, Lewis DR, Petkov VI, Penberthy L (2017) Cancer Epidemiol Biomarkers Prev 26(4):632–641. https://doi.org/10.1158/1055-9965.Epi-16-0520. Cancer Incidence and Survival Trends by Subtype Using Data from the Surveillance Epidemiology and End Results Program, 1992–2013

Odermatt A, Becker S, Khanna VK, Kurzydlowski K, Leisner E, Pette D, MacLennan DH (1998) Sarcolipin regulates the activity of SERCA1, the fast-twitch skeletal muscle sarcoplasmic reticulum Ca2+-ATPase. J Biol Chem 273(20):12360–12369. https://doi.org/10.1074/jbc.273.20.12360

Oikonomopoulou K, Diamandis EP, Hollenberg MD (2010) Kallikrein-related peptidases: proteolysis and signaling in cancer, the new frontier. Biol Chem 391(4):299–310. https://doi.org/10.1515/bc.2010.038

Paniagua-Herranz L, Moreno I, Nieto-Jiménez C, Garcia-Lorenzo E, Díaz-Tejeiro C, Sanvicente A, Doger B, Pedregal M, Ramón J, Bartolomé J, Manzano A, Gyorffy B, Gutierrez-Uzquiza Á, Pérez Segura P, Calvo E, Moreno V, Ocana A (2024) Genomic and Immunologic correlates in prostate Cancer with high expression of KLK2. Int J Mol Sci 25(4). https://doi.org/10.3390/ijms25042222

Peng Y, Greenland NY, Lang UE, Stohr BA (2022) LZTS2: A novel and independent prognostic biomarker for clear cell renal cell carcinoma. Pathol Res Pract 232:153831. https://doi.org/10.1016/j.prp.2022.153831

Popławski P, Bogusławska J, Hanusek K, Piekiełko-Witkowska A (2021) Nucleolar proteins and Non-Coding RNAs: roles in renal Cancer. Int J Mol Sci 22(23). https://doi.org/10.3390/ijms222313126

Prakash A, Paunikar S, Webber M, McDermott E, Vellanki SH, Thompson K, Dockery P, Jahns H, Brown JAL, Hopkins AM, Bourke E (2023) Centrosome amplification promotes cell invasion via cell-cell contact disruption and Rap-1 activation. J Cell Sci 136(21). https://doi.org/10.1242/jcs.261150

Rae F, Bulmer B, Nicol D, Clements J (1999) The human tissue Kallikreins (KLKs 1–3) and a novel KLK1 mRNA transcript are expressed in a renal cell carcinoma cDNA library. Immunopharmacology 45(1–3):83–88. https://doi.org/10.1016/s0162-3109(99)00059-4

Saunders W (2005) Centrosomal amplification and spindle multipolarity in cancer cells. Semin Cancer Biol 15(1):25–32. https://doi.org/10.1016/j.semcancer.2004.09.003

Shannon P, Markiel A, Ozier O, Baliga NS, Wang JT, Ramage D, Amin N, Schwikowski B, Ideker T (2003) Cytoscape: a software environment for integrated models of biomolecular interaction networks. Genome Res 13(11):2498–2504. https://doi.org/10.1101/gr.1239303

Shi J, Miao D, Lv Q, Wang K, Wang Q, Liang H, Yang H, Xiong Z, Zhang X (2023) The m6A modification-mediated OGDHL exerts a tumor suppressor role in CcRCC by downregulating FASN to inhibit lipid synthesis and ERK signaling. Cell Death Dis 14(8):560. https://doi.org/10.1038/s41419-023-06090-7

Shuch B, Amin A, Armstrong AJ, Eble JN, Ficarra V, Lopez-Beltran A, Martignoni G, Rini BI, Kutikov A (2015) Understanding pathologic variants of renal cell carcinoma: distilling therapeutic opportunities from biologic complexity. Eur Urol 67(1):85–97. https://doi.org/10.1016/j.eururo.2014.04.029

Siegel RL, Miller KD, Fuchs HE, Jemal A (2021) Cancer statistics, 2021. CA: A Cancer. J Clin 71(1):7–33. https://doi.org/10.3322/caac.21654

Song Z, Xue C, Wang H, Gao L, Song H, Yang Y (2024) Development of a centrosome amplification-associated signature in kidney renal clear cell carcinoma based on multiple machine learning models. Comput Biol Chem 115:108317. https://doi.org/10.1016/j.compbiolchem.2024.108317

Stegeman H, Span PN, Kaanders JH, Bussink J (2014) Improving chemoradiation efficacy by PI3-K/AKT Inhibition. Cancer Treat Rev 40(10):1182–1191. https://doi.org/10.1016/j.ctrv.2014.09.005

Sudo H, Maru Y (2007) LAPSER1 is a putative cytokinetic tumor suppressor that shows the same centrosome and midbody subcellular localization pattern as p80 Katanin. Faseb J 21(9):2086–2100. https://doi.org/10.1096/fj.06-7254com

Sudo H, Maru Y (2008) LAPSER1/LZTS2: a pluripotent tumor suppressor linked to the Inhibition of katanin-mediated microtubule severing. Hum Mol Genet 17(16):2524–2540. https://doi.org/10.1093/hmg/ddn153

Tan SK, Hougen HY, Merchan JR, Gonzalgo ML, Welford SM (2023) Fatty acid metabolism reprogramming in CcRCC: mechanisms and potential targets. Nat Rev Urol 20(1):48–60. https://doi.org/10.1038/s41585-022-00654-6

Tollervey D, Kiss T (1997) Function and synthesis of small nucleolar RNAs. Curr Opin Cell Biol 9(3):337–342. https://doi.org/10.1016/s0955-0674(97)80005-1

Venables KM, Upton JL, Hawkins ER, Tee RD, Longbottom JL, Newman Taylor AJ (1988) Smoking, atopy, and laboratory animal allergy. Br J Ind Med 45(10):667–671. https://doi.org/10.1136/oem.45.10.667

Vitre BD, Cleveland DW (2012) Centrosomes, chromosome instability (CIN) and aneuploidy. Curr Opin Cell Biol 24(6):809–815. https://doi.org/10.1016/j.ceb.2012.10.006

Wang Y, Luo M, Wang F, Tong Y, Li L, Shu Y, Qiao K, Zhang L, Yan G, Liu J, Ji H, Xie Y, Zhang Y, Gao WQ, Liu Y (2022) AMPK induces degradation of the transcriptional repressor PROX1 impairing branched amino acid metabolism and tumourigenesis. Nat Commun 13(1):7215. https://doi.org/10.1038/s41467-022-34747-y

Wettersten HI, Aboud OA, Lara PN Jr., Weiss RH (2017) Metabolic reprogramming in clear cell renal cell carcinoma. Nat Rev Nephrol 13(7):410–419. https://doi.org/10.1038/nrneph.2017.59

Wu T, Hu E, Xu S, Chen M, Guo P, Dai Z, Feng T, Zhou L, Tang W, Zhan L, Fu X, Liu S, Bo X, Yu G (2021) ClusterProfiler 4.0: A universal enrichment tool for interpreting omics data. Innov (Camb) 2(3):100141. https://doi.org/10.1016/j.xinn.2021.100141

Xia T, Zhang M, Lei W, Yang R, Fu S, Fan Z, Yang Y, Zhang T (2023) Advances in the role of STAT3 in macrophage polarization. Front Immunol 14:1160719. https://doi.org/10.3389/fimmu.2023.1160719

Xiao GF, Yan X, Chen Z, Zhang RJ, Liu TZ, Hu WL (2020) Identification of a novel Immune-Related prognostic biomarker and Small-Molecule drugs in clear cell renal cell carcinoma (ccRCC) by a merged Microarray-Acquired dataset and TCGA database. Front Genet 11:810. https://doi.org/10.3389/fgene.2020.00810

Xu C, Liang H, Zhou J, Wang Y, Liu S, Wang X, Su L, Kang X (2020) LncRNA small nucleolar RNA host gene 12 promotes renal cell carcinoma progression by modulating the miR–200c–5p/collagen type XI A1 chain pathway. Mol Med Rep 22(5):3677–3686. https://doi.org/10.3892/mmr.2020.11490

Xu Q, Chen S, Hu Y, Huang W (2021) Landscape of immune microenvironment under immune cell infiltration pattern in breast Cancer. Front Immunol 12:711433. https://doi.org/10.3389/fimmu.2021.711433

Yan C, Niu Y, Ma L, Tian L, Ma J (2022) System analysis based on the cuproptosis-related genes identifies LIPT1 as a novel therapy target for liver hepatocellular carcinoma. J Transl Med 20(1):452. https://doi.org/10.1186/s12967-022-03630-1

Yang W, Zhang K, Li L, Ma K, Hong B, Gong Y, Gong K (2020) Discovery and validation of the prognostic value of the LncRNAs encoding snornas in patients with clear cell renal cell carcinoma. Aging 12(5):4424–4444. https://doi.org/10.18632/aging.102894

Yoshimura T, Hamada T, Hijioka H, Souda M, Hatanaka K, Yoshioka T, Yamada S, Tsutsui M, Umekita Y, Nakamura N, Tanimoto A (2016) PCP4/PEP19 promotes migration, invasion and adhesion in human breast cancer MCF-7 and T47D cells. Oncotarget 7(31):49065–49074. https://doi.org/10.18632/oncotarget.7529

Zeng YJ (2019) AnnoProbe: annotate the gene symbols for probes in expression array. R package version 0.1.0

Zhang Y, Tian J, Qu C, Peng Y, Lei J, Sun L, Zong B, Liu S (2020) A look into the link between centrosome amplification and breast cancer. Biomed Pharmacother 132:110924. https://doi.org/10.1016/j.biopha.2020.110924

Zhang C, Ma X, Wei G, Zhu X, Hu P, Chen X, Wang D, Li Y, Ruan T, Zhang W, Tao K, Wu C (2023a) Centrosomal protein 120 promotes centrosome amplification and gastric cancer progression via USP54-mediated deubiquitination of PLK4. iScience 26(1):105745. https://doi.org/10.1016/j.isci.2022.105745

Zhang H, Wang N, Yu T, Li Q, Yang L, Su Y, Wang P, Liu J, Yang L, Zhang J (2023b) Bioinformatic analysis on the prognostic value of neurotransmitter Receptor-Related genes in kidney renal clear cell carcinoma. Altern Ther Health Med 29(8):356–365

Zhang S, Sun L, Cai D, Liu G, Jiang D, Yin J, Fang Y, Wang H, Shen Y, Hou Y, Shi H, Tan L (2023c) Development and validation of PET/CT-Based nomogram for preoperative prediction of lymph node status in esophageal squamous cell carcinoma. Ann Surg Oncol 30(12):7452–7460. https://doi.org/10.1245/s10434-023-13694-y

Zhang X, Chao P, Zhang L, Xu L, Cui X, Wang S, Wusiman M, Jiang H, Lu C (2023d) Single-cell RNA and transcriptome sequencing profiles identify immune-associated key genes in the development of diabetic kidney disease. Front Immunol 14:1030198. https://doi.org/10.3389/fimmu.2023.1030198

Zhang L, Zhang X, Guan M, Zeng J, Yu F, Lai F (2024) Machine-learning developed an iron, copper, and sulfur-metabolism associated signature predicts lung adenocarcinoma prognosis and therapy response. Respir Res 25(1):206. https://doi.org/10.1186/s12931-024-02839-6

Zhao JZ, Ye Q, Wang L, Lee SC (2021) Centrosome amplification in cancer and cancer-associated human diseases. Biochim Biophys Acta Rev Cancer 1876(1):188566. https://doi.org/10.1016/j.bbcan.2021.188566

Zhu L, Tian Q, Gao H, Wu K, Wang B, Ge G, Jiang S, Wang K, Zhou C, He J, Liu P, Ren Y, Wang B (2022) PROX1 promotes breast cancer invasion and metastasis through WNT/β-catenin pathway via interacting with HnRNPK. Int J Biol Sci 18(5):2032–2046. https://doi.org/10.7150/ijbs.68960

Publisher's note Springer Nature remains neutral with regard to jurisdictional claims in published maps and institutional affiliations.